Control of insulin granule formation and function by the ABC transporters ABCG1 and ABCA1 and by oxysterol binding protein OSBP

Syed Saad Hussain[a,†], Megan T. Harris[a,†], Alex J. B. Kreutzberger[b,c,‡], Candice M. Inouye[a], Catherine A. Doyle[a], Anna M. Castle[a], Peter Arvan[d], and J. David Castle[a,c,*]

[a]Department of Cell Biology, [b]Department of Molecular Physiology and Biological Physics, and [c]Center for Membrane and Cell Physiology, University of Virginia School of Medicine, Charlottesville, VA 22908; [d]Division of Metabolism, Endocrinology, and Diabetes, University of Michigan Medical School, Ann Arbor, MI 48105

ABSTRACT In pancreatic β-cells, insulin granule membranes are enriched in cholesterol and are both recycled and newly generated. Cholesterol's role in supporting granule membrane formation and function is poorly understood. ATP binding cassette transporters ABCG1 and ABCA1 regulate intracellular cholesterol and are important for insulin secretion. RNAi interference–induced depletion in cultured pancreatic β-cells shows that ABCG1 is needed to stabilize newly made insulin granules against lysosomal degradation; ABCA1 is also involved but to a lesser extent. Both transporters are also required for optimum glucose-stimulated insulin secretion, likely via complementary roles. Exogenous cholesterol addition rescues knockdown-induced granule loss (ABCG1) and reduced secretion (both transporters). Another cholesterol transport protein, oxysterol binding protein (OSBP), appears to act proximally as a source of endogenous cholesterol for granule formation. Its knockdown caused similar defective stability of young granules and glucose-stimulated insulin secretion, neither of which were rescued with exogenous cholesterol. Dual knockdowns of OSBP and ABC transporters support their serial function in supplying and concentrating cholesterol for granule formation. OSBP knockdown also decreased proinsulin synthesis consistent with a proximal endoplasmic reticulum defect. Thus, membrane cholesterol distribution contributes to insulin homeostasis at production, packaging, and export levels through the actions of OSBP and ABCs G1 and A1.

INTRODUCTION

In eukaryotic cells, sterols are essential membrane lipids that must be maintained within narrowly defined limits of concentration to support a wide array of functions both at the cell surface and intracellularly. Regulation of cholesterol in metazoa entails not only control of the overall level of free cholesterol through a combination of biosynthesis, import, storage, and export but also control of its subcellular distribution, which factors significantly in the distinct biophysical properties and unique functions of different membrane-bounded organelles (Chang *et al.*, 2006; van Meer *et al.*, 2008; Mesmin and Maxfield, 2009). In regulated secretory cells that store and secrete insulin, proinsulin is synthesized in the endoplasmic reticulum where membrane cholesterol content is low (~5 mol% of membrane lipid; van Meer *et al.*, 2008; Sokolov and Radhakrishnan, 2010). As folded proinsulin advances from the endoplasmic reticulum (ER) through the Golgi complex and into immature granules (where it is proteolytically processed to insulin for subsequent storage), membrane cholesterol levels progressively increase (Orci *et al.*, 1981). Fully packaged insulin is stored in granules whose surrounding membranes are estimated to contain ~35 mol%

cholesterol (Westhead, 1987), comparable to concentrations typically found in the plasma membrane (van Meer *et al.*, 2008; Mesmin and Maxfield, 2009). The typical pancreatic β-cell contains 9–10,000 insulin storage granules with a total surface area that is ~4.5 times that of the plasma membrane (Sato and Herman, 1981). Thus, the secretory granule pool contains a very large fraction of the β-cell's membrane cholesterol.

We have been interested in how cholesterol might be regulated and concentrated in membranes that are used for insulin granule formation. Although endocytic recycling and reutilization of granule membrane components postexocytosis certainly contributes to the formation of new insulin granules, it is clear that there must also be accompanying synthesis and incorporation of new membrane components. Indeed, under normoglycemic conditions, proinsulin synthesis is active (Wicksteed *et al.*, 2003) and is increased by feeding (Schuit *et al.*, 1988). Yet under these conditions, only a small fraction of the population of stored granules is mobilized and undergoes exocytosis (Rorsman and Renström, 2003). To maintain the β-cell's homeostatic level of insulin, there is continual turnover of granules by lysosomal degradation (Orci *et al.*, 1984; Marsh *et al.*, 2007; Riahi *et al.*, 2016), which increases as glucose concentrations decrease (Halban and Wolheim, 1980). Replacing the lost membranes is essential and requires a source of cholesterol and mechanisms to concentrate it. These considerations raise interesting possibilities about the roles of the oxysterol binding protein OSBP and the cholesterol-regulatory ABC (ATP binding cassette) transporters ABCG1 and ABCA1. OSBP localizes to interorganellar contact sites between the ER and *trans*-Golgi network (TGN; Storey *et al.*, 1998), where it enables nonvesicular cholesterol export from the ER and concentration in the TGN through coupled countertransport of phosphatidylinositol-4-phosphate (Mesmin *et al.*, 2013b, 2017). Although ABCs G1 and A1 have mainly been the focus of studies aimed at assessing their contributions to cholesterol export from the cell surface to extracellular lipoproteins (reviewed in Chang *et al.* [2006], Wang *et al.* [2007], Tarling and Edwards [2012], and Phillips [2014]), interest has grown in possible roles in regulating intracellular cholesterol distribution (Vaughan, 2005; Sturek *et al.*, 2010; Tarling and Edwards, 2011, 2012). In particular, our earlier study of the relationship of ABCG1 deficiency to impaired glucose tolerance and impaired insulin secretion in mice raised the possibility that ABCG1 might be an important player in regulating the distribution of cholesterol during insulin granule formation (Sturek *et al.*, 2010). To gain further insight into this earlier observation and to consider more broadly how intracellular cholesterol distribution might regulate insulin's secretory pathway, we have hypothesized that OSBP, ABCG1, and ABCA1 collaborate to support the continual and tightly controlled supply of cholesterol-enriched membranes that are needed for insulin granule biogenesis and exocytosis. Notably, there is strong reason to believe that increased cholesterol levels enhance the packaging and storage of secretory products (Blazquez *et al.*, 2000; Wang *et al.*, 2000; Hosaka, 2003), whereas conditions of either cholesterol excess or deficiency impair the regulated exocytosis of secretory granules (Brunham *et al.*, 2007; Hao *et al.*, 2007; Hao and Bogan, 2009; Xia *et al.*, 2008; Sturek *et al.*, 2010; Bogan *et al.*, 2012) including the formation of fusion pores (Kreutzberger *et al.*, 2015).

In the present study, we have examined small interfering RNA (siRNA)-mediated knockdowns of ABCG1, ABCA1, and OSBP. We find that deficiency of either ABCG1 or OSBP decreases the stability of newly formed insulin granules leading to increased loss due to lysosomal degradation, whereas a similar effect elicited by ABCA1 loss is more modest. Notably, deficiency of any of the three transporters reduces the competence for glucose-stimulated insulin secretion.

Further, our supporting evidence argues that OSBP and the ABC transporters act serially and that their mechanism is indeed linked to membrane cholesterol availability within the secretory pathway.

RESULTS

ABCG1 knockdown in INS1 cells reduces cellular insulin content

In undertaking these studies, ABCG1 was our initial focus due to our earlier efforts in exploring its role in insulin-secreting cells (Sturek *et al.*, 2010). At the outset, we improved on the specificity of the commercially available anti-ABCG1 antibody used previously by developing a new antibody to a synthetic peptide located in the cytoplasmic N-terminal domain (see *Materials and Methods*). This antibody was not useful for immunofluorescence but exhibited excellent selectivity in detecting ABCG1 by Western blotting, and we could confirm successful siRNA-mediated knockdown of transporter expression (Supplemental Figure S1). Within 48 h of initiating knockdown in the INS1-832/13 beta cell line and particularly after 72 h, levels of ABCG1 were reduced 80–90% (*Materials and Methods*). Notably, this caused a consistent, significant decrease in cellular insulin levels (Figure 1A).

Knockdown affects the products of proinsulin processing and other proteins of immature secretory granules

To explore the intracellular source of secretory protein loss in ABCG1-deficient cells, we mainly used the glucose-responsive insulin-secreting C-peptide-modified human proinsulin (GRINCH) clone of INS1 cells (Haataja *et al.*, 2013) that stably expresses human proinsulin containing a superfolder green fluorescent protein (GFP) insert in the C-peptide domain (hPro-CpepSfGFP). hPro-CpepSfGFP is synthesized, transported, processed, and insulin stored and secreted in parallel with endogenous proinsulin/insulin. The CpepSfGFP (endoproteolytic processing product) allows for easy monitoring of intracellular transport and secretion using both biochemical and fluorescence approaches. Knockdown of ABCG1 reduced the levels of CpepSfGFP present in cell lysates similar to its effect on insulin (Figure 1B). The level of the hPro-CpepSfGFP precursor protein was also significantly decreased, albeit to a lesser extent than that observed for CpepSfGFP.

To gain insight regarding which intracellular organelles might account for the loss of the CpepSfGFP granule marker, we subjected postnuclear supernatant fractions to a two-step isoosmotic cell fractionation procedure. Our goal was to resolve subpopulations of secretory granules based on subtle differences in buoyant density and to distinguish lower-density organelles involved in proinsulin transport and processing (see *Materials and Methods* and Figure 1C). Analysis of the U1, U2, L1, and L2 fractions by quantitative Western blotting showed that the ER chaperone calnexin was largely confined to U1. Carboxypeptidase E (CPE, involved in trimming the products of proinsulin cleavage by prohormone convertases and known to localize to TGN, immature and mature secretory granules; Dhanvantari and Loh, 2000) was abundant in U1 but also was well represented in U2 and L2. This is consistent with lower-density TGN-derived membranes being present in U1 and progressively higher-density immature granules (IGs) and mature secretory granules (SGs) being enriched in U2 and L2, respectively. Finally, CpepSfGFP, one of the final products of hPro-CpepSfGFP processing, was well represented in U1 and U2 (containing early stages of granule biogenesis) but was most abundant in L2 (that is enriched in mature insulin granules).

Application of this fractionation protocol to ABCG1 knockdown cells showed only modest changes to hPro-CpepSfGFP and CPE distributions but substantial loss of CpepSfGFP in the postnuclear
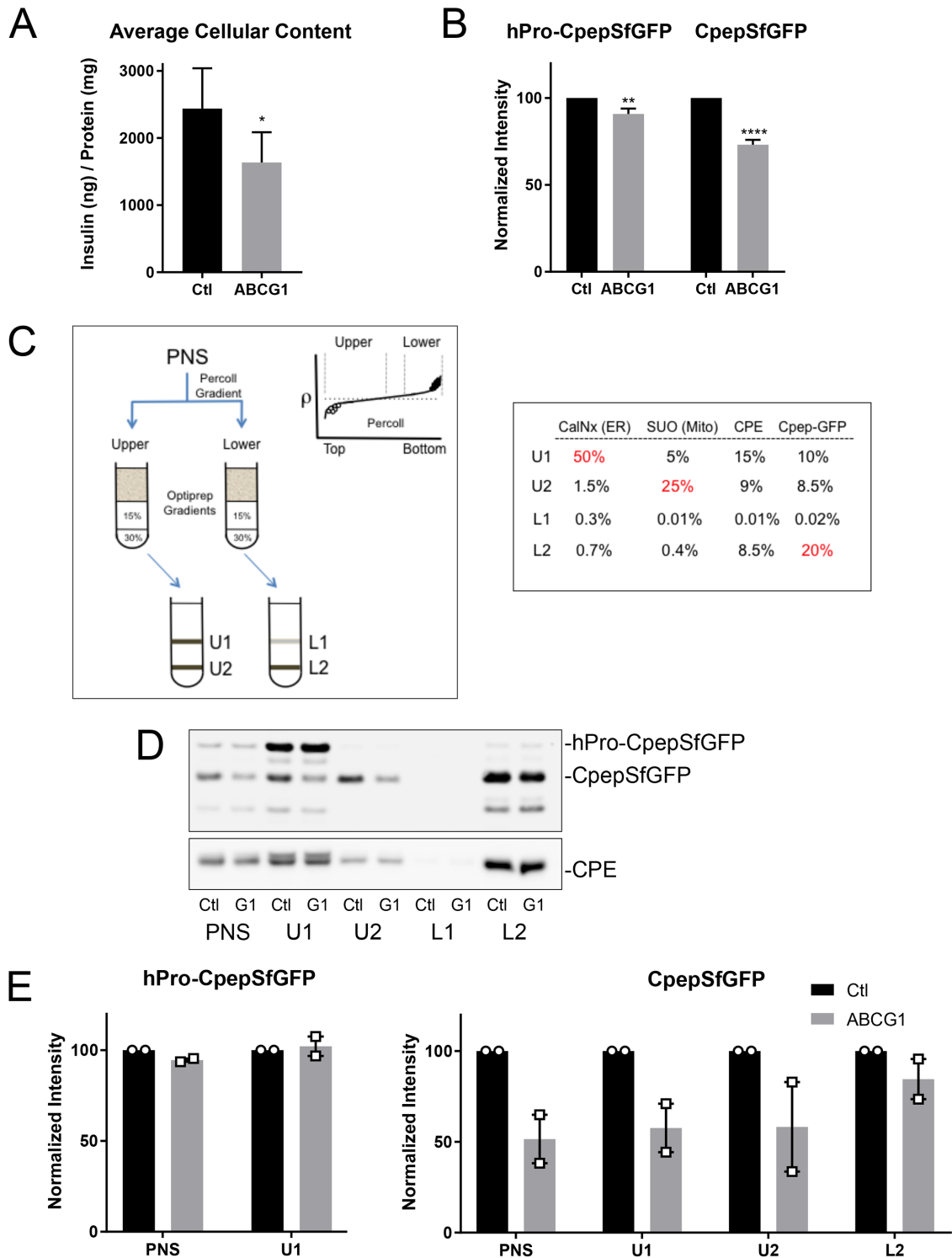
FIGURE 1: RNAi-mediated depletion of ABCG1 reduces the levels of secretory proteins in insulin-secreting cells and also inhibits stimulated secretion. (A) Levels of insulin in INS1 cells measured by ELISA following treatment with siRNA (control or ABCG1-targeted smart pool); $n = 7$. (B) Levels of hPro-CpepSfGFP and CpepSfGFP in GRINCH cells quantified from Western blots following control and ABCG1 knockdowns; $n = 20$. Data are presented as mean ± SEM. p values determined by Student's t test; *, $p < 0.05$; **, $p < 0.01$; ****, $p < 0.0001$. (C) Isoosmotic fractionation protocol used to resolve granule populations and accompanying distributions of marker proteins in the subfractions (PNS, postnuclear supernatant; U1, U2 and L1, L2) resolved on the iodixanol gradients from the upper (lower density) and lower (higher density) bands of the Percoll gradient, respectively. Markers are as follows: CalNx, calnexin (ER); SUO, succinate-ubiquinone oxidoreductase (mitochondria); CPE, carboxypeptidase (condensing vacuoles, immature and mature granules); Cpep-GFP, CpepSfGFP. Percentages in red show principal concentration sites. (D) Western blots showing the distributions of hPro-CpepSfGFP and CpepSfGFP (upper blot) and CPE (lower blot) in fractions obtained from parallel fractionation of control (Ctl) and ABCG1-depleted (G1) cells. As discussed in the text and shown in

supernatant (PNS), U1, and U2 fractions, with less apparent loss from the L2 fraction (Figure 1, D and E, and Supplemental Figure S2A). These data suggest that the main secretory pathway effect of ABCG1 is in influencing the retention of proinsulin processing products during granule biogenesis and maturation. Additionally, by analysis in continuous density sucrose gradients, two other secretory granule proteins, secretogranin III (Hosaka, 2003, 2005) and phogrin (Wasmeier and Hutton, 1996; Wasmeier et al., 2005), were also reduced in the ABCG1 knockdown cells, in parallel with losses of CpepSfGFP and a portion of CPE, whereas VAMP4 (associated predominantly with the TGN [Ahras et al., 2006; Hao and Bogan, 2009; Zhang et al., 2017]) was largely unaffected (Supplemental Figure S2B). These data further support that secretory granule protein loss is particularly prevalent during the period of granule maturation, distal to the exit of VAMP4 from secretory pathway membranes.

The ABCG1 knockdown effect is selective for newly formed granules, and RNA interference (RNAi)-resistant ABCG1 prevents their loss

Because β-cells contain a reservoir of long-lived mature granules that could predate and thus persist long after siRNA-mediated transfection, we decided to transiently transfect GRINCH cells to newly express a fluorescence-tagged secretory protein (NPY-mCherry, a very good marker for insulin granules; Supplemental Figure S3). The goal was to determine whether ABCG1 deficiency resulted in greater loss of the marker of newer granules than for the CpepSfGFP marker of both the newer and preexisting granule populations. Indeed, Western blotting of ABCG1 knockdown cells showed that loss of NPY-mCherry consistently and significantly exceeded the loss of CpepSfGFP (Figure 2A). To ensure that loss of newer granules specifically reflected deficiency in ABCG1, we first showed that an siRNA targeted to the 3′-untranslated region (UTR) of rat ABCG1 was effective in reducing CpepSfGFP levels (Figure 2B), and then we expressed the same siRNA along with NPY-mCherry in cell lines stably expressing either EGFP-tagged ABCG1 or a nonfunctional ABCG1(K124M) mutant (Kobayashi, 2006) that lacked the endogenous 3′-UTR. Both variants of ABCG1 showed very similar intracellular distributions, substantially concentrating at sites marked by the TGN markers proinsulin (undergoing condensation in forming SGs) and Golgin 97 (Figure 2C). Both EGFP-tagged constructs were resistant to siRNA-mediated knockdown, but only the wild-type EGFP-ABCG1 restored normal levels of NPY-mCherry (Figure 2D). Thus, the data suggest that functional ABCG1 preserves the stability of younger SGs. In making these findings, we point out that the distribution now shown for ABCG1 contradicts our previous claim that this transporter resides in insulin granules (Sturek et al., 2010). As discussed in a separate manuscript, this earlier diagnosis is in error; there is very little ABCG1 associated with insulin granules, and a major portion of this short-lived protein colocalizes with the TGN (Harris et al., unpublished data).

ABCG1 deficiency does not amplify unstimulated secretion but increases lysosomal degradation of proteins from the insulin secretory pathway

Two alternatives might explain the loss of proteins from the younger SGs observed in ABCG1-deficient cells: 1) increased routing during intracellular transport along unstimulated secretory pathway(s)

(Kuliawat and Arvan, 1992; Turner and Arvan, 2000; Tsuchiya et al., 2010; Cao et al., 2013; Holst et al., 2013; Du et al., 2016) or 2) targeting to lysosomes for degradation (Marsh et al., 2007; Hannemann et al., 2012; Goginashvili et al., 2015; Riahi et al., 2016; Hummer et al., 2017; Zhang et al., 2017). We found that the level of unstimulated secretion of hPro-CpepSfGFP over 20 h (at 5.5 mM glucose) was essentially unaffected by ABCG1 knockdown, and the level of unstimulated secretion of CpepSfGFP was not increased whatsoever (and indeed appeared slightly lower than that of control cells; Figure 3A). Further, immunofluorescence localization of proinsulin and VAMP4 in ABCG1-deficient cells showed both to be highly concentrated in the perinuclear cytoplasm as in control cells, consistent with a close association with the TGN (Figure 3B). Together, these results are not consistent with increased unstimulated secretion and dispersion of IGs throughout the cytoplasm as in cells lacking PICK1 and HID1 (Cao et al., 2013; Du et al., 2016). In addition, they contrast with the profound dispersion of the TGN observed in INS1 cells deficient in BAIAP3 (Zhang et al., 2017). However, during the final 24 h of knockdown, when we added to the medium leupeptin, pepstatin, and antipain, which are endocytosed and delivered to lysosomes, there was a significantly increased recovery of CpepSfGFP as well as a smaller increase in hPro-CpepSfGFP (Figure 3C). In support of secretory protein loss by lysosomal degradation, we noted in the Western blot at the bottom of Figure 3C that the lower-molecular-weight band below CpepSfGFP (about the size of SfGFP) was significantly increased in the presence of lysosomal inhibitors, suggesting that this band may be an intermediate in the degradation of CpepSfGFP within lysosomes. This interpretation is further supported by pulse-chase labeling studies showing that the band appears kinetically after proinsulin processing (see below) but is never detected in the secretion (Supplemental Figure S8).

Interestingly, the presence of this low-molecular-weight band in the control cells indicates that a portion of proinsulin/C-peptide is normally being delivered to lysosomes. A previous study reported similar continual degradation and implicated ongoing macroautophagy (Riahi et al., 2016). Accordingly, we carried out immunostaining of our cells with an antibody against LC3, a widely used marker for this process. Although we observed a positive signal, it was quite modest and certainly was not increased in ABCG1-deficient cells (unpublished data). Thus, it seems most likely that the secretory protein loss we have observed is occurring by a lysosomal pathway that is distinct from macroautophagy.

Exogenous cholesterol addition partially alleviates the loss of CpepSfGFP to lysosomal degradation when added to ABCG1-deficient cells

In previous studies of pancreatic islets, we found that addition of exogenous cholesterol 1 d in advance of testing glucose-stimulated insulin secretion was able to partially overcome inhibition that resulted from knockout of ABCG1 (Sturek et al., 2010). We wondered whether a similar low concentration (20 μM) of exogenous cholesterol delivered as a methyl β-cyclodextrin (MβCD) complex might also reduce the loss of CpepSfGFP that we observed following knockdown of ABCG1 in GRINCH cells. As shown in Figure 3D, addition of cholesterol during the final day of knockdown indeed partially restored CpepSfGFP in ABCG1-depleted cells. In attempting to increase the

---

Figures 3C and 6C, the band running below CpepSfGFP appears to be an intermediate in the degradation of CpepSfGFP in lysosomes. (E) Two separate fractionations documenting little or no loss of hPro-CpepSfGFP in PNS and U1 but pronounced loss of CpepSfGFP in PNS, U1, and U2 as compared with L2 following ABCG1 knockdown as quantified from Western blots. Supplemental Figure S2 documents similar loss for CPE but no loss of SUO or CalNx in ABCG1-depleted samples.
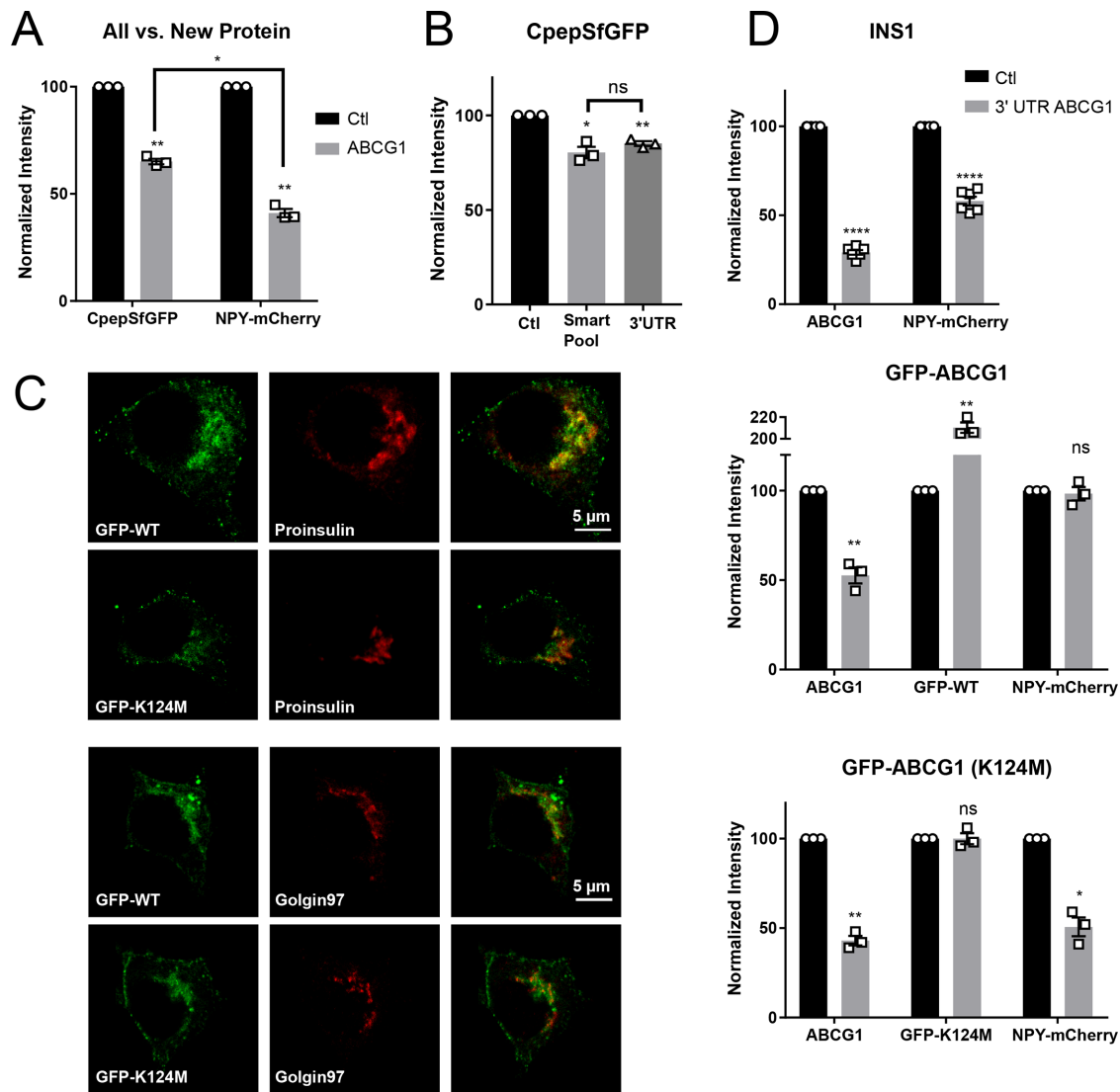
FIGURE 2: RNAi-mediated knockdown of ABCG1 causes preferential loss of newly produced secretory protein and the effect reflects a deficiency in ABCG1. (A) Loss of NPY-mCherry (new protein), expressed during the last 24 h of knockdown, is significantly greater than the loss of CpepSfGFP (all protein), a portion of which was present before inducing the knockdown. Quantification from Western blots; $n = 3$. (B) Comparable loss of CpepSfGFP when siRNA targeted to the 3'-UTR of ABCG1 is substituted for the siRNA smart pool. Quantification from Western blots; $n = 3$. (C) Fluorescence images showing extensive (but not full) colocalization of stably expressed N-terminally tagged GFP-ABCG1 and of the nonfunctional Walker domain mutant GFP-ABCG1(K124M) with concentrated proinsulin and the *trans*-Golgi marker Golgin97. (D) Loss of NPY-mCherry caused by siRNA targeted to the 3'-UTR of ABCG1 occurs in control INS1 cells; $n = 6$. Loss is averted in INS1 cells stably expressing a low level of GFP-ABCG1 chimera lacking the 3'-UTR but not when the cells express nonfunctional GFP-ABCG1(K124M). Quantification from Western blots; $n = 3$. Data are presented as means ± SEM. p values are determined by Student's t test; *, $p < 0.05$; **, $p < 0.01$; ****, $p < 0.0001$.

observed CpepSfGFP recovery, we found that neither increasing cholesterol to 50 µM nor extending the 20 µM treatment to 48 h provided added benefit. Notably, neither 20 nor 50 µM exogenous cholesterol changed cellular levels of free cholesterol (Supplemental Figure S4A).

Biosynthetic pulse-chase labeling demonstrates early loss of insulin and CpepSfGFP in nascent SGs and rescue by exogenous cholesterol

Expression of NPY-mCherry during the time of ABCG1 knockdown highlighted an effect on newer granules. To learn how closely coupled the loss of secretory proteins was to insulin granule formation, we used pulse-chase biosynthetic labeling with ^{35}S-amino acids to track the fate of newly synthesized secretory and lysosomal proteins comparatively in ABCG1-deficient cells. Knockdown of ABCG1 in INS1 cells, did not alter the amount of proinsulin synthesized or the rate of prohormone processing, indicating no effect of ABCG1 deficiency at the level of the ER or during proinsulin transit through the Golgi. However, the level of insulin that accumulated in the ABCG1-deficient cells was notably diminished (Figure 4A). In contrast, procathepsin B trafficking and processing was unaffected in ABCG1-deficient cells (Figure 4B). Additionally,
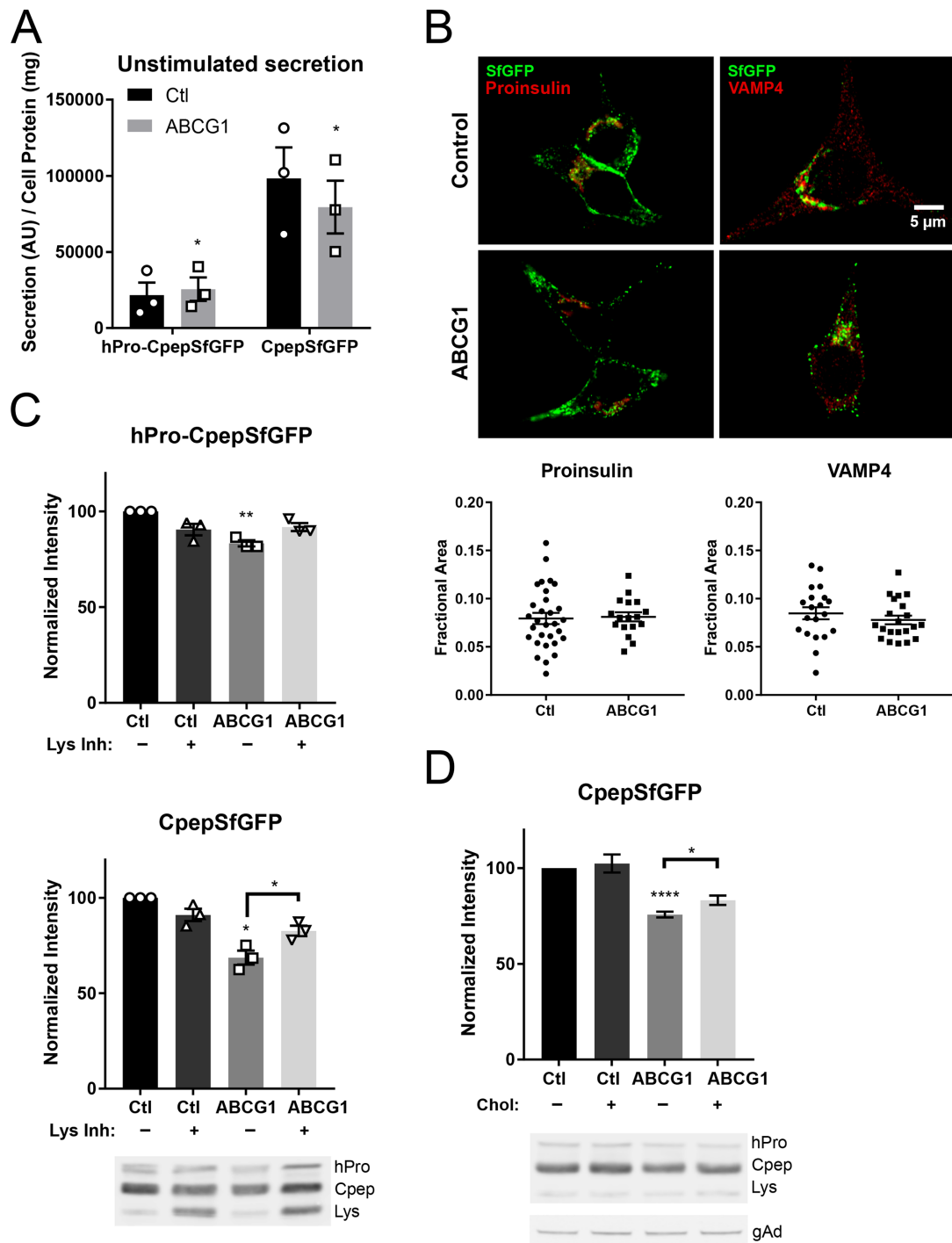
FIGURE 3: Deficiency of ABCG1 does not increase unstimulated secretion of hPro-CpepSfGFP or CpepSfGFP but instead causes loss of CpepSfGFP by lysosomal degradation. The loss is attenuated by adding exogenous cholesterol during knockdown. (A) Secreted hPro-CpepSfGFP and CpepSfGFP (normalized to cell protein) by ABCG1-deficient cells is similar to or slightly less than that observed for control knockdown cells that were incubated for 20 h without stimulation. Quantification from Western blots; $n = 3$. (B) Knockdown of ABCG1 does not alter the intracellular distribution of proinsulin or VAMP4 immunostaining. Quantification shows that the perinuclear area occupied by proinsulin or VAMP4 fluorescence is unchanged (control cells, # = 30 [proinsulin], # = 20 [VAMP4]; ABCG1 cells, # = 17 [proinsulin], # = 21 [VAMP4]). (C) Loss of hPro-CpepSfGFP and CpepSfGFP induced by depletion of ABCG1 is diminished by endocytic uptake of lysosomal enzyme inhibitors during the final portion of RNAi-mediated knockdown. Quantification from Western blots; $n = 3$. The accompanying representative image shows the bands for hPro-CpepSfGFP (hPro) and CpepSfGFP (Cpep) as well as the lower-molecular-weight band (Lys) that is a putative intermediate in the lysosomal degradation of CpepSfGFP. (D) Exogenous cholesterol (20 µM) added during the final day of knockdown of ABCG1 decreases the loss of CpepSfGFP. Quantification from Western blots; $n = 5$. The accompanying representative image shows the same bands as in C; an example image of γ-adaptin used for normalization in all experiments (see *Materials and Methods*) is shown at the bottom. Data are presented as mean ± SEM. p values are determined by Student's t test; *, $p < 0.05$; **, $p < 0.01$; ****, $p < 0.0001$.
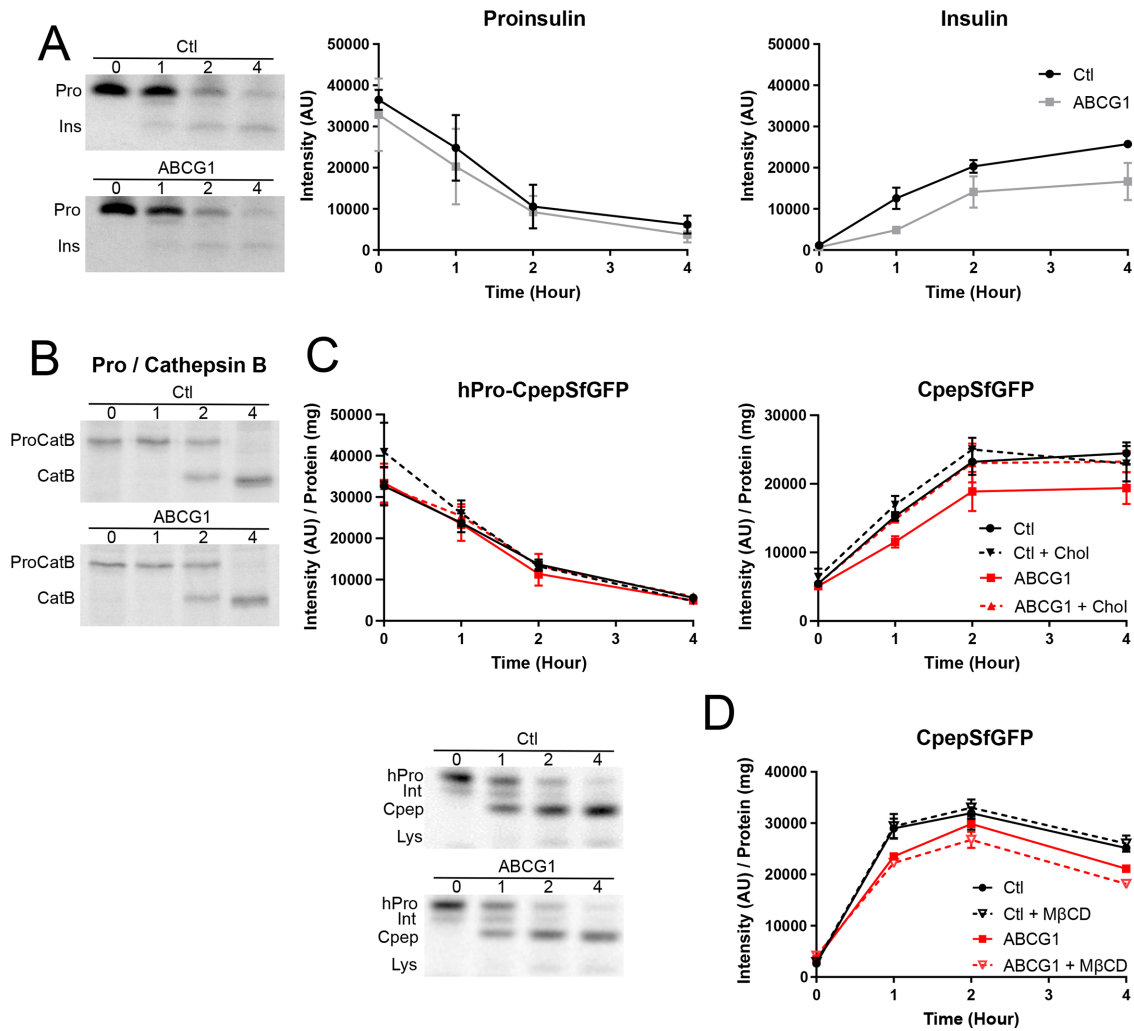
FIGURE 4: Effects of ABCG1 knockdown on granule formation. (A) Production and processing of ^{35}S-amino acid–labeled proinsulin are not affected by depletion of ABCG1 in INS1 cells. Representative phosphorimage comparing labeled proinsulin/insulin in control and ABCG1 knockdown cells. Quantitative results pooled from three experiments (0–2 h chase; extended to 4 h chase in two of the experiments) show that accumulation of labeled insulin during granule formation is noticeably decreased by ABCG1 knockdown. (B) Transport and processing of procathepsin B (to cathepsin B in lysosomes) is not affected by ABCG1 knockdown. The phosphorimage is representative of two separate experiments. (C) Tracking of hPro-CpepSfGFP and CpepSfGFP in GRINCH cells following pulse labeling with ^{35}S-amino acids. Representative phosphorimage shows the progressive processing of hPro-CpepSfGFP (hPro) through an intermediate (Int) to CpepSfGFP (Cpep) as well as accumulation of a lysosomal degradation band (Lys) in control and ABCG1 knockdown samples. Quantification shows no effect of ABCG1 knockdown or of cholesterol-MβCD addition on the level and processing of hPro-CpepSfGFP. For CpepSfGFP, levels are significantly decreased by ABCG1 knockdown starting at 1 h ($p < 0.05$). Rescue of CpepSfGFP levels by cholesterol-MβCD addition (ABCG1 + chol) is indicated by no significant difference from control (starting at 1 h) and significant difference ($p < 0.05$) from ABCG1 (starting at 2 h). (D) Addition of MβCD alone significantly increases the loss of CpepSfFP in ABCG1-deficient samples by 2 h (results for hPro-CpepSfGFP mimic those in C [unpublished data]). Significance determined by two-way analysis of variance (ANOVA); $n = 3$ in C and in D. Data are presented as mean ± SEM.

unstimulated secretion of newly synthesized proinsulin, insulin, and procathepsin B was not elevated in the ABCG1-deficient cells (not shown). Similarly, in ABCG1-deficient cells the synthesis and processing of hPro-CpepSfGFP appeared unaffected, but there was a clear deficit in the accumulation of newly synthesized CpepSfGFP (Figure 4C). Once again, there was no increase in unstimulated secretion of newly synthesized CpepSfGFP (not shown but consistent with the results of Figure 2A). Taken together, the data indicate that inefficient recovery of newly made insulin and C-peptide occurs

intracellularly within ~2 h postsynthesis at a stage corresponding to young SGs, with the remaining products appearing thereafter to be stable for granule storage.

Because rescue of total cellular CpepSfGFP levels by exogenous cholesterol in ABCG1-deficient cells may have been limited by the presence of long-lived mature SGs that preceded transporter knockdown, we made use of the pulse-chase biosynthetic labeling approach to assess the effects of exogenous cholesterol selectively on nascent granules. Addition of 20 μM cholesterol-MβCD had no

effect on the levels or processing of hPro-CpepSfGFP, but this treatment fully restored newly synthesized CpepSfGFP in ABCG1-deficient cells (Figure 4C). Importantly, addition of MβCD alone caused no recovery of CpepSfGFP but instead slightly aggravated its loss (Figure 4D). These data strongly suggest that a cholesterol imbalance perturbs the stability of young insulin SGs.

The effects of ABCA1 deficiency on new granule formation are smaller than for ABCG1 and are not significantly affected by addition of cholesterol-MβCD or MβCD alone

A series of previous studies have shown that ablation of ABCA1 in mouse pancreatic islets inhibits glucose-stimulated insulin secretion (Brunham et al., 2007; Sturek et al., 2010; Kruit et al., 2011, 2012). Therefore, we tested whether deficiency in this transporter also affects the formation of insulin granules in GRINCH cells. Initially, we compared the distributions of ABCA1 and ABCG1 using subcellular fractionation on sucrose density gradients centrifuged to equilibrium and found that they were quite similar (Supplemental Figure S5B). Then, using our pulse-chase biosynthetic labeling approach, we compared parallel siRNA-mediated knockdowns of ABCA1, ABCG1, and both transporters together against the same control knockdown used in the ABCG1 experiments above. As shown in Figure 5A, 80–90% deficiency in ABCA1 (see Materials and Methods; sample Western blot, Supplemental Figure S5A) had no effect on the synthesis and processing of hPro-CpepSfGFP but had a similar

but smaller effect on the loss of CpepSfGFP as compared with ABCG1. The decrease in level of labeled CpepSfGFP in ABCA1 knockdowns as compared with the control was observed throughout the timecourse but only reached significance ($p < 0.05$) at 1 h. Interestingly, combined knockdown of ABCs G1 and A1 had an effect on CpepSfGFP that was not significantly different from that observed in the knockdown of ABCG1 alone throughout the timecourse. The lack of additive or synergistic effects argues that the functions of the two transporters are not redundant, yet contribute toward the same goal of forming stable granules.

In a separate set of experiments, we also found that addition of either cholesterol-MβCD or MβCD alone during the final day of RNAi-mediated knockdown of ABCA1 did not significantly alter the level of labeled CpepSfGFP as compared with the unsupplemented ABCA1 knockdown, although inclusion of MβCD alone showed a slight tendency toward aggravation of CpepSfGFP loss (Figure 5B). Together, these data suggest that although the two transporters may have complementary functions, the formation of new insulin granules relies to a greater extent on ABCG1 than on ABCA1.

OSBP deficiency causes loss of both CpepSfGFP and hPro-CpepSfGFP by affecting granule formation as well as proinsulin synthesis in the ER

The ability of exogenous cholesterol to decrease the loss of young insulin granules by lysosomal degradation in ABCG1-deficient cells suggests that ABCG1 facilitates the concentrating of cholesterol in nascent granule membranes and that exogenous cholesterol may bypass its deficiency. To extend these observations, we sought to interfere with the delivery of endogenous cholesterol to the TGN, where ABCG1 is accumulated and where granule formation begins, in order to determine whether this also compromised the formation of stable insulin granules. OSBP has gained wide interest as it has been implicated in robust nonvesicular transport of cholesterol from the ER to increase its level in the TGN (Mesmin et al., 2013a,b, 2017). As in other cell types, OSBP localizes in GRINCH cells at TGN-associated foci that are prospective sites of cholesterol delivery (Figure 6A, left). These foci are adjacent to concentrated proinsulin staining and in close proximity to IGs marked by both proinsulin staining and SfGFP (Figure 6A, right). Also a portion of the Q_B-SNARE Vti1a (which in part marks IGs [Walter et al., 2014]) concentrates at or near sites marked by OSBP (unpublished data). These distributions are consistent with OSBP localizing to ER–TGN contacts shown by electron microscopy to be adjacent to forming granules (e.g., Figure 2 in Oliver and Hand, 1983). Remarkably, RNAi-mediated knockdown of OSBP caused a significant decrease in the steady-state level of CpepSfGFP and at the same time decreased the steady-state level of hPro-CpepSfGFP more robustly than observed for ABCG1 knockdown (Figure 6B). These effects were confirmed using a different
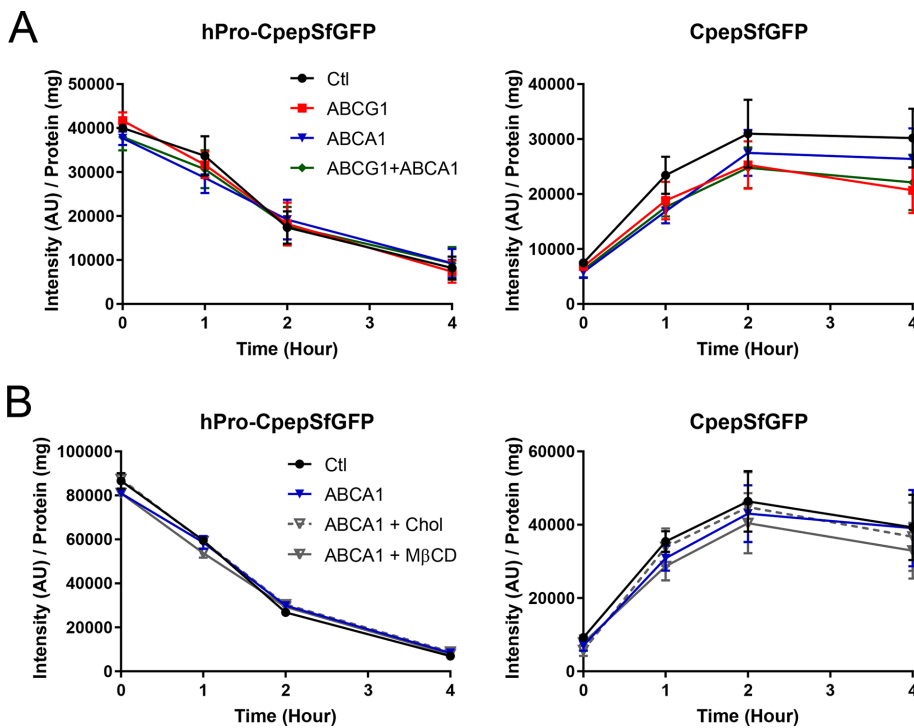
FIGURE 5: Effects of ABCA1 knockdown as compared with knockdowns of ABCG1 and of ABCs G1 and A1 in combination. Tracking of hPro-CpepSfGFP and CpepSfGFP in GRINCH cells during chase incubation following pulse labeling with ^{35}S-amino acids as in Figure 4C. (A) Quantification shows no effect on the level and processing of hPro-CpepSfGFP (left). ABCA1 knockdown does not decrease CpepSfGFP as much as in ABCG1 knockdown, and ABCG1/A1 combined knockdown does not significantly decrease CpepSfGFP beyond the level observed in ABCG1 knockdown alone (right). CpepSfGFP levels in ABCA1 knockdown samples are significantly less than in control ($p < 0.05$) only at 1 h. Significance determined by two-way ANOVA; $n = 5$. (B) Cholesterol-MβCD addition does not affect the small loss of CpepSfGFP observed in ABCA1-deficient samples. Addition of MβCD alone slightly, but not significantly, aggravates the loss of CpepSfGFP in ABCA1-deficient samples; $n = 2$. Data are presented as mean ± SEM.

siRNA, which was directed to the 3′-UTR of OSBP mRNA, and in cells depleted of OSBP using this approach, we were able to achieve partial rescue by expressing OSBP-mCherry (Supplemental Figure S6). As shown in Figure 6C, at least some of the decrease of both hPro-CpepSfGFP and CpepSfGFP could be restored by coincubation of knockdown cells with lysosomal inhibitors (which again increased the GFP-positive degradation product). These data indicate that as in the case of ABCG1, the activity of OSBP has a significant impact on the biogenesis and stability of young insulin SGs. The more robust and likely proximal effect of OSBP (as compared with ABCG1) depletion is supported by a significantly altered fluorescence localization of hPro-CpepSfGFP/CpepSfGFP in
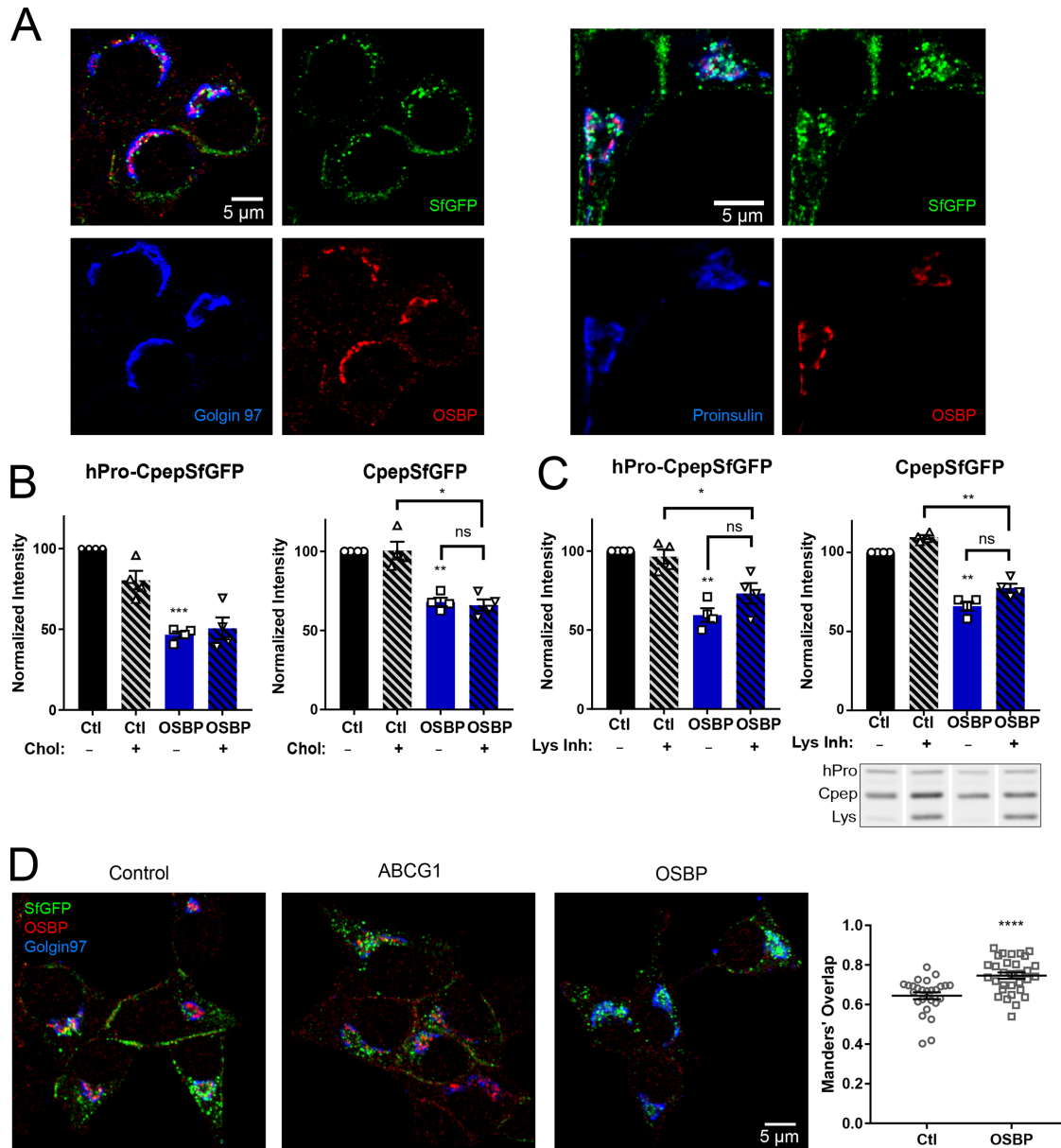
FIGURE 6: Effects of OSBP depletion on hPro-CpepSfGFP and CpepSfGFP. (A) OSBP immunostaining is concentrated in puncta that colocalize at the TGN with Golgin 97 (left) and are closely apposed to proinsulin (right). SfGFP mainly marks insulin granules and overlaps proinsulin (cyan) in young granules. Specificity of OSBP staining documented in Supplemental Figure S6. (B) Steady-state levels of both hPro-CpepSfGFP and CpepSfGFP are significantly decreased in OSBP knockdown cells as compared with control knockdown cells and are not restored by exogenous cholesterol. Quantification from Western blots; n = 4. (C) Endocytic uptake of lysosomal inhibitors partially restores both hPro-CpepSfGFP (hPro) and CpepSfGFP (Cpep) and increases the lysosomal SfGFP degradation product (Lys) in OSBP-depleted samples. The included image shows a representative Western blot (noncontiguous lanes are from the same blot). Quantification from Western blots; n = 4. (D) Images showing distinct separation of SfGFP fluorescence and Golgin97 immunostaining in control and ABCG1 knockdowns but increased overlap in OSBP knockdowns. Accompanying plot shows Manders' overlap; control cells, # = 26; OSBP KD cells, # = 31. Data are presented as mean ± SEM; p values are determined by Student's t test; *, p < 0.05; **, p < 0.01; ***, p < 0.001; ****, p < 0.0001.

OSBP-depleted cells such that SfGFP significantly overlaps with Golgin97 (Figure 6D).

The finding that the steady-state level of hPro-CpepSfGFP was decreased also raised the possibility that OSBP depletion might have effects in the ER. Consequently, we used pulse-chase/immunoprecipitation to examine the synthesis of new hPro-CpepSfGFP. Remarkably, in OSBP-depleted cells, hPro-CpepSfGFP synthesized during the pulse labeling was significantly decreased. Thereafter, hPro-CpepSfGFP appeared to be processed at the same rate as in control cells, suggesting no effect on ER-to-Golgi and intra-Golgi proinsulin transport (Figure 7A). When the pulse period was shortened (to 10 min) to negate any potential contribution from ER-associated degradation (ERAD), the inhibition of hPro-CpepSfGFP synthesis remained apparent in OSBP-deficient cells (Figure 7B). Moreover, MG132 addition preceding and during pulse labeling did not enhance recovery of hPro-CpepSfGFP (Figure 7B), further supporting our deduction that OSBP deficiency does not diminish newly synthesized hPro-CpepSfGFP levels via ERAD but instead causes a decrease in proinsulin translation itself.

Elevated cholesterol in the ER can decrease coupled translation/translocation of nascent polypeptides (Nilsson et al., 2001). None of the knockdowns—ABCG1, ABCA1, ABCs G1 and A1 together, and OSBP—caused a significant change in the total level of cellular free cholesterol measured using an oxidation and peroxidase-coupled fluorometric assay (Supplemental Figure S4B; Robinet et al., 2010). Nevertheless, OSBP deficiency might lead to a modest local accumulation of cholesterol in the ER due to decreased transport to the TGN (Nishimura et al., 2013; Mesmin et al., 2017). To evaluate this possibility, we examined cholesterol biosynthesis, which is well known to be quite sensitive to elevated ER cholesterol (Goldstein and Brown, 2015). Whereas incorporation of [^{3}H]acetate into cholesterol (Yamauchi et al., 2015) was only modestly decreased by ABCG1 depletion, it was robustly inhibited by OSBP depletion (Figure 7C), consistent with a modest degree of ER cholesterol accumulation.

In addition to the biosynthetic defect observed in OSBP-depleted cells, the final level of CpepSfGFP that accumulated during chase was significantly reduced (Figure 7A), which we confirmed by normalizing our data in the control and OSBP-depleted samples to the same initially synthesized level of hPro-CpepSfGFP (Supplemental Figure S7). Further, similar to the effect seen in ABCG1-deficient cells (Figure 4C), this loss was confined to newly made granules during the first 2 h after synthesis (Figure 7A). Thus, OSBP deficiency resulted in both diminished newly synthesized hPro-CpepSfGFP and decreased accumulation of CpepSfGFP in mature storage granules, leading us to conclude that OSBP activity may help to couple proinsulin production and insulin packaging, potentially through ER-to-TGN movement of cholesterol.

In an attempt to build support for the suspected elevation of ER cholesterol inferred from suppressed cholesterol biosynthesis upon OSBP depletion, we looked for redistribution of cholesterol away from the perinuclear region where the TGN is localized. Thus, we examined control and OSBP knockdown GRINCH cells that had been fixed and stained with filipin using fluorescence microscopy (Maxfield and Wüstner, 2012). For quantification, we followed recently presented strategies and measured fluorescence that accumulated in perinuclear regions of interest known to contain both TGN and the endosomal recycling compartment (ERC) and also normalized to total cell fluorescence (Mesmin et al., 2017). We found that there was a modest decrease in perinuclear fluorescence suggesting that cholesterol in the TGN might be lower in OSBP-depleted cells, but when normalized to total cell fluorescence, the decrease did not reach significance (Figure 7D). Also, we were un-

able to detect increased diffuse cytoplasmic fluorescence surrounding perinuclear accumulations, suggesting that the increase in ER cholesterol is likely to be only modest. Similarly, knockdowns of ABCG1 and ABCA1 did not detectably alter perinuclear filipin fluorescence (unpublished data). These data are consistent with milder effects on endocrine granule formation than has been seen upon blockade of cholesterol biosynthesis and uptake (Wang et al., 2000).

Loss of hPro-CpepSfGFP and CpepSfGFP caused by OSBP deficiency is not rescued by exogenous cholesterol, and combined knockdowns of OSBP and ABCG1 and ABCA1 do not have an additive effect
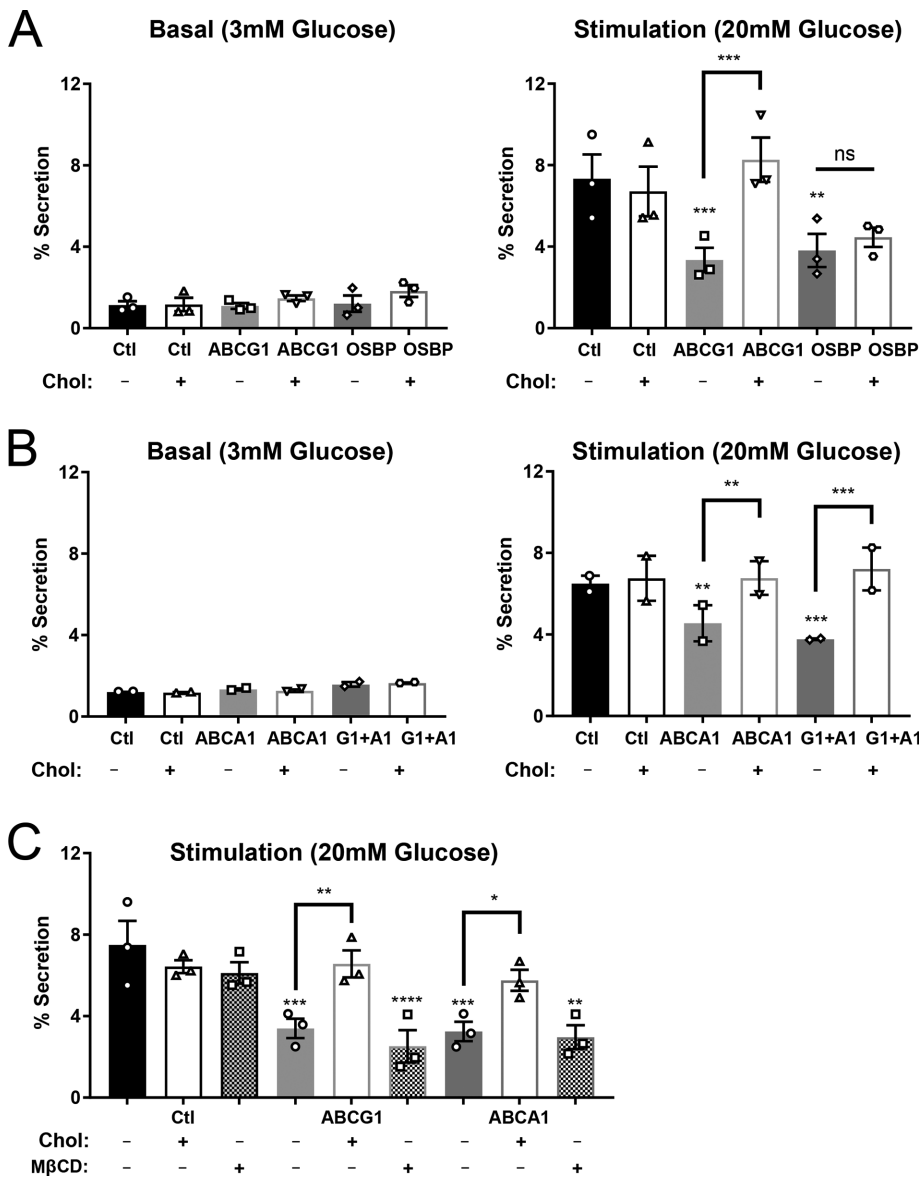
The decrease in both hPro-CpepSfGFP and CpepSfGFP caused by OSBP depletion led us to examine how adding exogenous cholesterol might affect the loss of the two proteins. If cholesterol levels are elevated in the ER as a result of OSBP knockdown, we were curious whether additional cholesterol might further decrease the synthesis of hPro-CpepSfGFP. On the other hand, if exogenous cholesterol addition stablizes young granules, we wondered whether it would recover some of the loss of CpepSfGFP. As shown in Figure 6B, the addition of exogenous cholesterol had no effect on the level of either protein. We also used our pulse-chase format to examine cholesterol's effect on biosynthesis of hPro-CpepSfGFP and the ensuing accumulation of CpepSfGFP. Even at a concentration of 50 μM cholesterol addition, biosynthesis was not further depressed and recovery of accumulating CpepSfGFP was not improved (Figure 7A). Finally, we carried out combined knockdowns of ABCG1 and OSBP and found that the effects on loss of CpepSfGFP did not exceed those observed with the individual knockdowns (Figure 7E). Likewise, knockdown of ABCA1 and OSBP together did not increase loss (unpublished data). These outcomes are consistent with OSBP and the two ABC transporters acting serially within the same pathway.

Glucose-stimulated exocytosis is decreased in ABCG1-, ABCA1-, and OSBP-deficient cells; exogenous cholesterol restores secretion only for ABCG1 and ABCA1 deficiency

Our and others' previous studies using pancreatic islets from ABCG1 and ABCA1 knockout mice showed that loss of either transporter inhibited glucose-stimulated insulin secretion (Brunham et al., 2007; Sturek et al., 2010; Kruit et al., 2011, 2012). Thus, we were interested whether depletion of ABCG1, ABCA1, or of OSBP would affect the glucose-stimulated secretory response in GRINCH cells. The presence of SfGFP-tagged protein enabled use of a facile and sensitive fluorescence assay for determining fractional release into the medium (Supplemental Figure S8; Zhu et al., 2016). As can be seen in Figure 8, A and B, exocytosis in response to stimulation by 20 mM glucose was indeed significantly decreased in ABCG1-, OSBP-, ABCA1-, and dual ABCG1/A1-deficient cells. Evaluation of secretion as a percent of total SfGFP fluorescence compensates for any loss of secretory protein due to lysosomal degradation. Thus, the deficiencies in these transporters inhibit secretion above and beyond the effects on production of stable granules. Strikingly, 20 μM exogenous cholesterol added during the final day of knockdown fully recovered secretion of SfGFP-tagged protein to control levels in ABCG1-deficient cells, quite similar to the previously observed cholesterol-induced recovery in ABCG1 knockout islets (Sturek et al., 2010). Cholesterol-MβCD addition also recovered secretion in ABCA1-deficient cells and in cells that were deficient in both ABCs G1 and A1. However, cholesterol-MβCD had no effect on OSBP-deficient GRINCH cells (Figure 8, A and B). Moreover, addition of MβCD alone had no
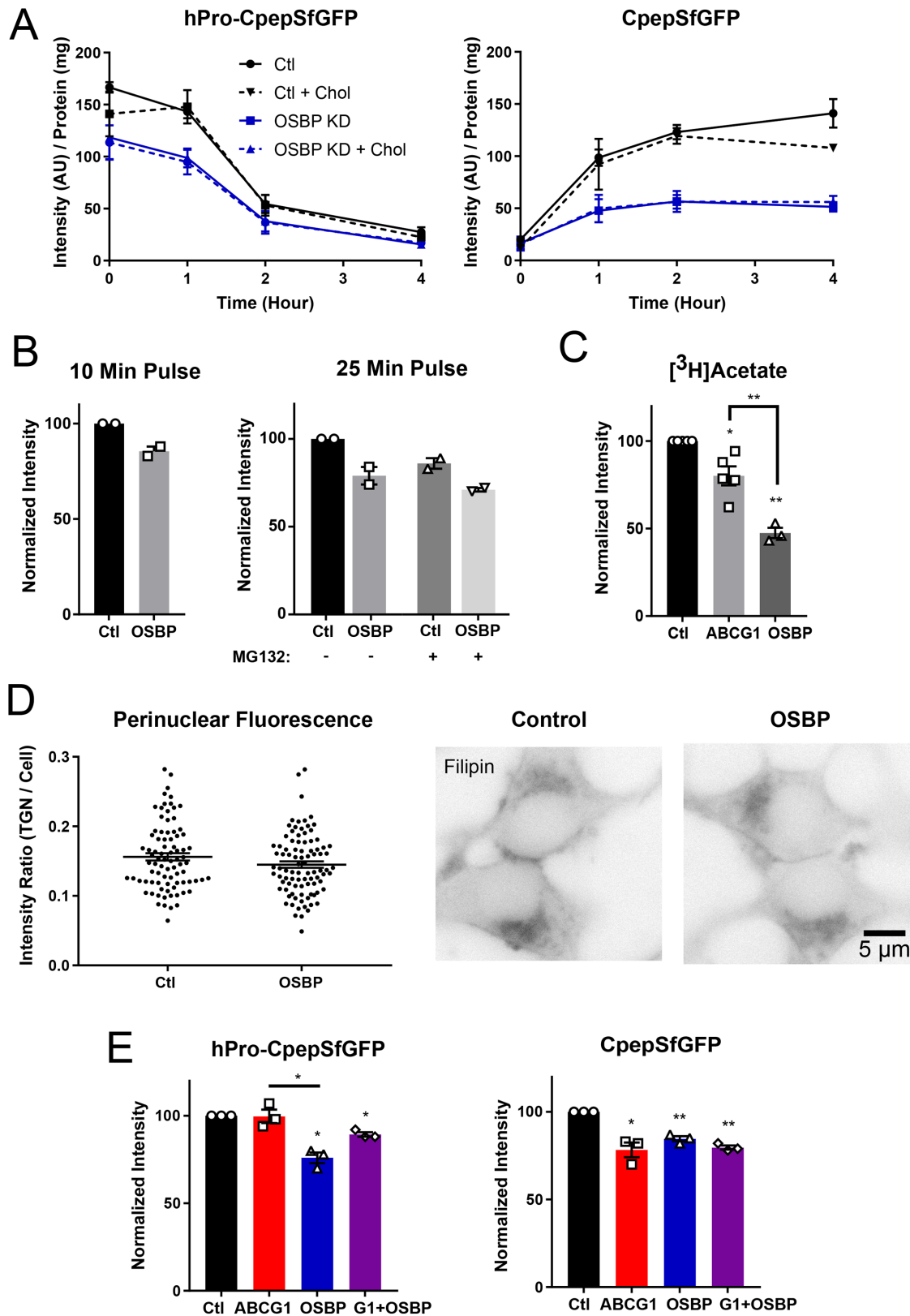
FIGURE 7: OSBP depletion reduces synthesis of hPro-CpepSfGFP and decreases CpepSfGFP accumulation but does not amplify the effects of ABCG1 knockdown. (A) Effect of OSBP knockdown and pretreatment with exogenous cholesterol on biosynthetically labeled hPro-CpepSfGFP and CpepSfGFP. hPro-CpepSfGFP levels in OSBP KD (+/− cholesterol) are significantly different from control (+/− cholesterol) at 0 and 1 h. CpepSfGFP levels (+/− cholesterol) are significantly different in OSBP KD from control (+/− cholesterol) at 1 h and later. Significance determined by two-way ANOVA; $n = 3$. (B) Neither shortening the labeling period (left) nor including the proteasomal inhibitor MG132 (right) affects the level of accumulation of hPro-CpepSfGFP. Data (intensity/mg protein) are normalized to the control

A Basal (3mM Glucose) | Stimulation (20mM Glucose)

B Basal (3mM Glucose) | Stimulation (20mM Glucose)

C Stimulation (20mM Glucose)

FIGURE 8: Glucose-stimulated secretion measured by release of fluorescence (SfGFP) is inhibited in cells depleted of ABCG1 or OSBP (A) and ABCA1 and combined ABCs G1 and A1 (B). Addition of 20 μM cholesterol-MβCD restores output in ABCG1-, ABCA1- and ABCG1/A1-depleted samples but not in OSBP-depleted samples. n = 3 (A); n = 2 (B). (C) In contrast to addition of cholesterol-MβCD, addition of MβCD alone does not rescue stimulated secretion; n = 3. Western blot images (Supplemental Figure S8) illustrate the proteins contributing to the fluorescent signal in secretion and cell lysates. Significance was determined by one-way ANOVA. Data are presented as mean ± SEM. *, p < 0.05; **, p < 0.01; ***, p < 0.001; ****, p < 0.0001.

cells might seem surprising given that exocytosis-defective granules were likely produced in advance of cholesterol addition. However, these findings are consistent with previous observations indicating that newly made granules are released in preference to older granules following glucose stimulation (Rhodes and Halban, 1987; Duncan et al., 2003; Michael et al., 2007) and that it was mainly these younger granules, whose glucose-stimulated insulin secretion was restored.

DISCUSSION

Our studies have made a strong case that ABCG1, ABCA1, and OSBP all act in the secretory pathway of pancreatic beta cells where they regulate the production, storage, and glucose-stimulated discharge of insulin and C-peptide. The hierarchical (OSBP proximal to ABCs G1 and A1) and likely collaborative function of these transporters is implicated by the differing degrees to which individual deficiencies affect proinsulin production and new insulin granule formation, yet the common and nonsynergistic effects of these deficiencies on exocytosis. Indeed, loss of OSBP affects proinsulin synthesis and impairs granule formation and secretion. ABCG1 loss affects only granule formation and secretion, whereas ABCA1 loss only modestly affects granule formation but impairs secretion to the same extent as ABCG1 loss. The inability of exogenous cholesterol to overcome any of the effects of OSBP depletion is consistent with a central role of OSBP in transporting endogenous cholesterol from the ER to the TGN, which may be essential for matching the levels of proinsulin synthesis and stable storage of its processed products. Whereas this possibility would reflect OSBP's key role in ER-TGN cholesterol transport (Mesmin et al., 2017), our conclusions that defects due to loss of OSBP are specifically related to cholesterol trafficking must be tempered by our inability to detect significant cholesterol red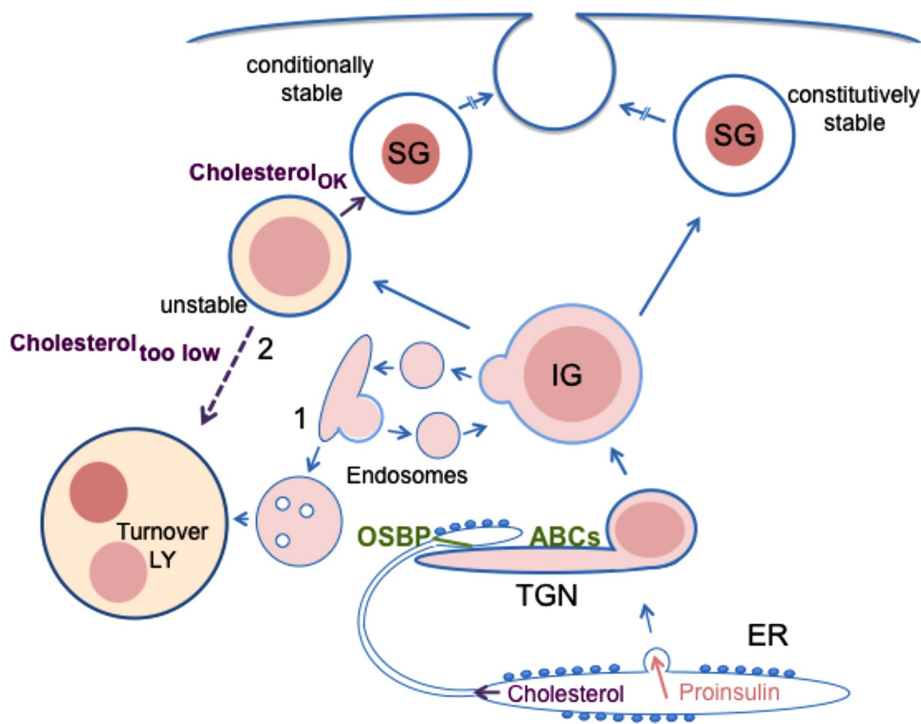istribution (Figure 7D). For several reasons, however, we believe that impaired cholesterol transport likely underlies the observed OSBP deficiency phenotype. First, OSBP knockdown results in both reduced biosynthesis of cholesterol (Figure 7C) and

restorative effect on inhibited secretion caused by transporter loss, implicating a specific cholesterol requirement (Figure 8C). The thorough recovery observed in ABCG1 and ABCA1 knockdown

(n = 2, each in duplicate). (C) Cholesterol biosynthesis as measured by [3H]acetate incorporation showing a slight decrease in ABCG1-depleted cells and strong decrease in OSBP-depleted cells. Quantification from scintillation counting of [3H]cholesterol separated by thin-layer chromatography; n = 3–5. (D) Modest but not significant decrease in filipin fluorescence concentrated perinuclearly in OSBP KD as compared with control. Fixed and stained cells are shown in reverse contrast to highlight perinuclear fluorescence, which was quantified and normalized to total cell fluorescence; control cells, # = 84; OSBP KD cells, # = 91 cells. Significance determined by Student's t test. (E) Combined knockdown of ABCG1 and OSBP does not increase the loss of CpepSfGFP beyond the level observed with either knockdown alone. Quantification from Western blots; n = 3. Data are presented as mean ± SEM; p values are determined by Student's t test; *, p < 0.05; **, p < 0.01.

FIGURE 9: Model of regulatory role of cholesterol dynamics in the insulin secretory pathway. During proinsulin synthesis and vesicular transport from the ER, there is parallel nonvesicular transport of cholesterol from the ER to the TGN that is mediated by OSBP acting at interorganellar contacts. Cholesterol transport along this pathway simultaneously aids in maintaining the low cholesterol content of the ER and provides cholesterol that is essential for supporting the normal level of stable insulin granule formation. At the TGN, ABCG1- and ABCA1-driven phospholipid translocation and cholesterol redistribution to the inner membrane leaflet promotes formation of new cholesterol-enriched membranes of nascent insulin granules. Deficiency in either OSBP or ABCG1 augments lysosomal degradation of young insulin granules, whereas deficiency of ABCA1 has a smaller effect at this level. The possible pathways of granule degradation (1 vs. 2) are discussed in the text. Exogenous cholesterol suppresses degradation in ABCG1-deficient cells but not in OSBP-deficient cells. The total granule pool that has escaped lysosomal degradation is nevertheless still affected by deficiency of ABCG1, ABCA1, or OSBP as indicated by their diminished exocytosis upon glucose stimulation.

loss of newly formed granules, the loss is quite minor plus it does not amplify the loss observed with ABCG1 depletion and is not altered by exogenous cholesterol addition (Figure 5). Yet, impaired exocytosis is rescued by cholesterol in ABCA1-depleted cells (Figure 8), implying that ABCA1 does indeed contribute to exocytotic competence in a cholesterol-dependent manner. We believe that the functions of OSBP, ABCG1, and ABCA1 are concentrated along the secretory pathway axis with a focus in beta cells at the TGN site where insulin granule formation begins (Figures 2C and 6A and Supplemental Figure S5). We thus hypothesize that OSBP and the two ABC transporters act serially to supply an essential TGN-associated cholesterol pool and utilize it, along with other membrane lipids, for concentration in cholesterol-enriched new granule membranes (Figure 9).

Although each of the three transporters may affect TGN cholesterol, we believe that the loss of secretory protein caused by transporter deficiency most likely occurs distally and involves IGs. Perturbations induced by transporter depletion have no effect on the processing or unstimulated secretion of proinsulin and do not appear to alter the granule budding process (Figures 3A and 4B). This contrasts with previous findings where ablation of other proteins involved in insulin granule formation such as PICK1, HID1, Rab2a, and BAIAP3 either delay or inhibit processing, delocalize poorly condensed granules throughout the cytoplasm, and significantly increase unstimulated proinsulin secretion (Cao *et al.*, 2013; Du *et al.*, 2016; Matsunaga *et al.*, 2017; Zhang *et al.*, 2017). Instead, our findings argue that cholesterol-insufficient young granules are lost through degradation in lysosomes, a fate that has been observed for other deficiencies (Hummer *et al.*, 2017; Zhang *et al.*, 2017).

There are two pathways that could account for lysosomal targeting. First, reduced cholesterol might decrease retention of secretory cargoes as well as membrane-associated proteins like CPE and result in their increased redistribution via AP-1 or other routes leading to endosomes and lysosomes (Edwards *et al.*, 2009; Sumakovic *et al.*, 2009; Hannemann *et al.*, 2012; Topalidou *et al.*, 2016). Second, newly formed granule membranes with suboptimal cholesterol content may be unstable because they are unable to fully condense and package their secretory contents. Higher internal osmotic activity could cause bilayer packing defects and/or decreased association with intragranular proteins (Blazquez *et al.*, 2000; Dhanvantari and Loh, 2000; Hosaka, 2003) or granule stabilizing proteins like calcium-activated protein for secretion (CAPS; Speidel *et al.*, 2008) and lead to lysosomal fusion rather than persistent storage. At present, we cannot fully distinguish between these possibilities, but we have observed no cholesterol-mediated defects in procathepsin B sorting or trafficking in ABCG1-deficient beta cells (Kuliawat and Arvan, 1994; Kuliawat *et al.*, 2004; Klumperman *et al.*, 1998), implying that neither recycling

redistribution of SfGFP fluorescence within the Golgi/TGN region (Figure 6D), which, respectively, are consistent with cholesterol accumulation in the ER and decreased levels in the TGN. Second, because granule formation proceeds at an attenuated level in each kind of transporter-deficient cell, we anticipate that the extent of cholesterol reduction in the TGN and IGs is much less drastic than in cells challenged with acute severe cholesterol deficiency (Wang *et al.*, 2000). Third, in our previous study of ABCG1 deficiency (Sturek *et al.*, 2010), we observed that cholesterol content of granule-enriched fractions of pancreatic MIN6 cells was decreased ~10%. Unfortunately, in the current studies of GRINCH cells, we have been unsuccessful in preparing fractions of newly formed insulin granules that are sufficiently pure to enable direct assessment of their cholesterol content unfettered by other organellar contaminants.

For ABCG1, our data are compelling that exogenous cholesterol overcomes its loss and averts both increased degradation of new insulin granules and impaired glucose-stimulated secretion. Although other explanations may be possible, the simplest explanation is that ABCG1 acts directly in facilitating cholesterol concentration to stabilize forming granule membranes and to ensure exocytotic competence. For ABCA1, our data suggest less direct involvement in distributing cholesterol; although ABCA1 depletion also causes a

of sorting receptors nor AP-1 mediated trafficking for lysosomal biogenesis is perturbed (Figure 4B). We are inclined to favor the second pathway because loss includes membrane and membrane-associated proteins (phogrin and CPE) as well as major secretory cargoes, insulin and secretogranin III (Figure 1 and Supplemental Figure S2). Also, the density distribution of remaining granule markers in ABCG1-deficient cells is unchanged from that of control cells (Supplemental Figure S2).

Macroautophagy is thought to proceed continually in β-cells (Riahi et al., 2016). Because levels of LC3-immunostained puncta are not increased, knockdown of OSBP or ABCG1 does not appear to enhance young granule macroautophagy. Rather, deficiency-related granule loss appears superimposed on other turnover mechanisms, and might possibly reflect a form of crinophagy wherein young insulin granules fuse directly with lysosomes (Orci et al., 1984), a process augmented under starvation conditions (Goginashvili et al., 2015) in which cholesterol supply could be limiting. Further studies are needed to resolve the pathway of enhanced young granule turnover in transporter-deficient cells.

Constitutive export pathways require cholesterol (Grimmer et al., 2005) at levels that are higher than in the TGN (Klemm et al., 2009; Hankins et al., 2015). Further, cholesterol deprivation profoundly alters secretory granule formation (Dhanvantari and Loh, 2000; Wang et al., 2000; Gondre-Lewis, 2006; Tsuchiya et al., 2010). Until now, neither ABCG1 nor ABCA1 has been implicated in these processes, and the view has been that cholesterol enrichment and concurrent sphingolipid synthesis in the TGN enable spontaneous (passive) assembly of cholesterol-enriched membranes by a thermodynamic trapping process (Holthuis and Menon, 2014). So why might these transporters have a role in the present context? We suggest that this reflects the need for both new granule membrane synthesis as well as efficient packaging of very highly concentrated secretory contents at low osmotic activity. As highlighted in the *Introduction*, β-cells invest a very large amount of membrane in storage of insulin, and at least a portion is regularly lost by lysosomal digestion. Although compensatory recycling following previous rounds of exocytosis contributes at least some of the membrane used to make new granules (Solimena et al., 1996; Arnaoutova et al., 2003; Bauer et al., 2004; Kuliawat et al., 2004; Vo et al., 2004; Wasmeier et al., 2005; Bäck et al., 2010; Walter et al., 2014; Zhang et al., 2017), there may be compositional editing and rerouting of cholesterol and sphingolipids during endocytosis as reported elsewhere (Mobius et al., 2003; Devlin et al., 2010; Kanerva et al., 2013). Thus, new input may be necessary even to restore and maintain recycled membranes. What ABCG1 and ABCA1 may provide is the ability to generate *new* cholesterol/sphingolipid-enriched membranes by promoting coordinate sphingomyelin synthesis and cholesterol translocation and concentration in the forming intragranular membrane leaflet. For this process, OSBP would serve as cholesterol source and as facilitator of ceramide delivery for sphingomyelin synthesis because activity of the ceramide transporter CERT is coupled to OSBP (Perry and Ridgway, 2006; Peretti et al., 2008). Both ABCs G1 and A1 have been implicated as floppases that translocate phosphatidylserine (PS) and phosphatidylcholine (PC) from the cytosolic to the luminal leaflet of the bilayer (Kobayashi, 2006; Sano et al., 2007; Quazi and Molday, 2013) and also drive cholesterol translocation (Pomorski et al., 2004; Vaughan, 2005; Phillips, 2014). Because ABCG1 seems directly related to providing cholesterol for forming new granule membranes (Figure 4), we speculate that it catalyzes translocation of phospholipid (likely PS) to the luminal leaflet; the consequent increase in cholesterol's chemical potential in the cytoplasmic leaflet would cause its redistribution to the luminal leaflet. Ensuing ret-

rotranslocation of PS via TGN-associated aminophospholipid flip-pase action (Zachowski et al., 1989; Ansari et al., 2015; Hankins et al., 2015) would increase cholesterol's chemical potential in the luminal leaflet, leading it to form condensed complexes with sphingolipids on the inner leaflet. Thus, we postulate that cholesterol delivered to the cytoplasmic leaflet by OSBP could be driven by ABCG1 to the luminal leaflet, allowing for its concentration during new granule membrane formation. We further speculate that translocation of PC to the luminal leaflet by ABCA1 provides substrate along with ceramide delivered by CERT for synthesizing sphingomyelin and enabling its concentration by condensation with the translocated cholesterol. We believe this could explain the less direct role of ABCA1 in forming new cholesterol-enriched granule membranes and the subtler phenotype of ABCA1 depletion on new granule stability. Moreover, this explanation could rationalize why exogenous cholesterol addition (which presumably increases the chemical potential of cholesterol in the TGN) is sufficient to bypass ABCG1 deficiency effects on young insulin granule stability with little effect on ABCA1 deficiency. Although this scenario seems plausible, we note that our hypothesis contrasts with prior views that these ABC transporters act elsewhere to limit, rather than promote, formation of cholesterol-enriched membranes (Vaughan, 2003, 2005; Zhu et al., 2008; Frechin et al., 2015; Ito et al., 2015; Yamauchi et al., 2015). The key difference may be *intra*compartmental cholesterol relocation coupled to phospholipid synthesis (for granule membranes) rather than *inter*compartmental cholesterol relocation (either intracellularly to the ER [Vaughan, 2003, 2005; Yamauchi et al., 2015] or extracellularly at the plasma membrane [Phillips, 2014]) without accompanying phospholipid synthesis.

Regarding perturbation of exocytosis, knockdowns of ABCG1, ABCA1, or OSBP each cause partial impairment (Figure 8), thus milder than when cholesterol is acutely depleted or its biosynthesis severely perturbed (Wang et al., 2000; Tsuchiya et al., 2010). This suggests that cholesterol management by these transporters represents a modulatory mechanism to adjust cholesterol beyond the existing levels in the TGN that support constitutive secretion. Because transporter-deficient cells still produce some new granules that have escaped lysosomal degradation yet are compromised in exocytotic efficiency (Figure 8), we presume these granules have compositional differences as compared with normal granules. Interestingly, our dual phenotype of granule loss to lysosomal degradation and impaired exocytosis is shared by insulin granules in beta cells lacking CAPS (Speidel et al., 2008), a protein that has been implicated in docking/priming of neuroendocrine granules at the plasma membrane in advance of exocytosis (Grishanin et al., 2002; Hammarlund et al., 2008; Liu et al., 2010; Kabachinski et al., 2016). It will be of great future interest to determine whether changes in membrane composition resulting from ABC or OSBP knockdown may decrease association of CAPS or other proteins that stabilize granules and function in exocytosis.

As a final issue, we acknowledge that earlier reports have shown that knockouts of ABCG1 and ABCA1 cause overaccumulation of insulin (Brunham et al., 2007; Sturek et al., 2010; Kruit et al., 2012) and also in the case of ABCA1, MβCD alone rather than cholesterol-MβCD rescued impaired exocytosis in islet β-cells (Kruit et al., 2011). These findings differ from our results where acute knockdown in beta cell lines caused a deficit of insulin and CpepSfGFP. Moreover, our current studies report that cholesterol-MβCD, not MβCD alone, rescued glucose-stimulated secretion caused by loss of ABCG1 and ABCA1 (Figure 8). More work is needed to determine whether embryological absence of these transporters leads to compensatory genetic changes that may alter/elevate intracellular cholesterol

(in the case of ABCA1 [Kruit et al., 2012]) and significantly impact on secretory granule formation, trafficking, and stability.

Taken together, our findings regarding the serial action of OSBP and ABCs G1 and A1 point to a cholesterol-dependent role of these transporters in regulating the insulin secretory pathway (Figure 9). Although many other metabolites are also critical regulators of proinsulin synthesis and insulin exocytosis, we conclude from our current work that cholesterol concentrations throughout the secretory pathway appear to couple the level of proinsulin synthesized with the creation of stable young insulin granules that are stored for future glucose-stimulated release.

MATERIALS AND METHODS
Reagents
MβCD, cholesterol-MβCD complex (soluble cholesterol), and lysosomal inhibitors (leupeptin, pepstatin, antipain) were from Sigma-Aldrich; proteasomal inhibitor MG132 was from Cayman Chemical Co.; Optiprep (iodixanol) was from Axis-Shield/Accurate Chemical; Percoll was from Amersham Biosciences.

Cells and culture
INS1 823/13 cells (Hohmeier et al., 2000) were maintained in RPMI 1640 medium, 10 mM HEPES, 1 mM sodium pyruvate, 50 μM β-mercaptoethanol, 1× pen/strep, and 10% fetal bovine serum (FBS; Atlanta Biological). GRINCH cells stably expressing hPro-CpepSf-GFP derived and clonally selected from INS1 823/13 cells described in Haataja et al. (2013) were obtained from the laboratory of coauthor Peter Arvan, University of Michigan Medical School. They were maintained in the same medium as parent INS1 cells but in the presence of neomycin.

Antibodies used for Western blotting, immunoadsorption, and immunofluorescence
CPE, mouse Mab, BD Transduction 610758; mitochondrial succinate–ubiquinone oxidoreductase (OxPhos complex II) mouse Mab, Abcam 14715; calnexin, rabbit, Enzo ADI-SPA-865F; mCherry, rabbit, Biovision 5993; GFP, for IPs, Life Technologies mouse Mab, 3E6; for Western blots, Santa Cruz B2, sc9996; γ-adaptin, BD Transduction mouse Mab 610386; cathepsin B, rabbit 06-480 (lot 23784), Upstate Cell Signaling; porcine insulin, guinea pig, Dako A0564; rat proinsulin, mouse Mab, ALPCO; phogrin, rabbit against N-terminus, gift of Christina Wasmeier and John Hutton (University of Colorado Medical Center, Denver, CO), and PTP 1A-2b, goat, Santa Cruz sc30337; VAMP4, rabbit, Affinity Bioreagents PA1-768; vti1a, guinea pig, Synaptic Systems 165005; secretogranin III, rabbit, gift of M. Hosaka, Akita Prefectural University, Japan; LIMP2, mouse Mab, gift of I. Sandoval, CBM Severo Ochoa, Spain; anti-ABCA1, rabbit, gift of John Parks, Wake Forest School of Medicine via our previous study (Sturek et al., 2010); specificity documented in Supplemental Figure S5A; OSBP, rabbit, ThermoFisher PA5-30110, lot PC1833132H and Sigma HPA039227, lot A106684.

For anti-ABCG1, commercial antibodies did not perform well on pancreatic cells containing relatively low amounts of antigen. Therefore, we developed a different ABCG1 anti-peptide antibody. Both synthetic peptide (C)KKVDNNFTEAQRFSSLPRR-NH$_2$ (within the N-terminal cytoplasmic domain) and rabbit polyclonal antibody were made by Pacific Immunology. The antibody was affinity purified using peptide coupled to Sulfolink (Pierce/ThermoFisher). Western blot (Supplemental Figure S1) shows very good specificity and loss of antigen upon RNAi-mediated knockdown in INS1 cells. However, the antibody is not satisfactory for immunofluorescence because the signal is unaffected by the same RNAi-mediated knockdown.

Secondary antibodies for immunofluorescence were Alexa conjugated from Molecular Probes/Life Technologies and Jackson Immunoresearch (species cross-adsorbed). When pairing other antibodies with guinea pig anti-insulin, use of secondary antibodies cross-adsorbed against guinea pig was essential. Secondary antibodies for Western blotting were from Licor: goat anti-rabbit 696, goat anti-mouse 800, and donkey anti-goat 800.

Procedure for siRNA knockdowns
For RNAi-mediated knockdowns, INS1 or GRINCH cells were transfected using the lipofectamine RNAiMax transfection reagent (Invitrogen/ThermoFisher) using a reverse transfection procedure. Complexes of 50 pmol siRNA/lipofectamine were generated in OptiMEM and incubated 30 min at room temperature in 35-mm dishes. Cells suspended in antibiotic-free growth medium (1 × 10^6 per dish) were added to complexes and cultured 48 h. At 48 h, medium was changed to standard growth medium; at 72 h cells were used for experiments. siRNAs were Dharmacon ON-TARGETplus.

1. Control (Ctl) ON-TARGETplus Non-targeting Pool (D-001810-10)
2. ABCG1 ON-TARGETplus Rat ABCG1 SMARTpool (GeneID 85264; Cat# L-093864-02)
3. ABCG1 3′-UTR-ON-TARGETplus Custom Duplex

   Sense AGGCAAAACCGGAGAAGAAUU

   Antisense 5′-P-UUCUUCUCCGGUUUUGCCUUU

4. ABCA1 ON-TARGETplus Mouse ABCA1 (GeneID 11303; Cat# J-040248-11-0005)
5. OSBP ON-TARGETplus Rat OSBP SMARTpool (GeneID 365410; Cat# L-085377-02)
6. OSBP 3′-UTR - ON-TARGETplus Custom Duplex

   Sense GGGCUUGAGUAUUGAGUUAUU

   Antisense 5′-P- UAACUCAAUACUCAAGCCCUU

Assessment of the extent of knockdown was performed by Western blotting on all experiments and ranged from 83 ± 9% (SD), $n = 20$ for ABCG1; 90 ± 5% (SD), $n = 16$ for ABCA1; and 77 ± 8% (SD), $n = 12$ for OSBP except where specifically noted. Also, the control siRNA routinely used did not significantly affect the steady-state levels of endogenous and GFP-tagged exogenous proteins that we routinely quantified in cell lysates (as compared with the levels in untreated cell lysates). Where lysosomal inhibitors were included during the final 24 h of knockdown, we added 10 μM leupeptin, 10 μM antipain, and 5 μM pepstatin, similar to Sirkis et al. (2013). Where exogenous cholesterol was added during the final 24 h of knockdown, final concentrations of 20 and 50 μM MβCD-cholesterol (soluble cholesterol) were added as specified. Under these conditions, there was no evidence of cytotoxicity as has been reported when higher concentrations are used (Tsuchiya et al., 2010). MβCD alone (20 μM) was added in the same manner.

Expression of NPY-mCherry during RNAi-mediated knockdown
To label newly formed insulin granules, we expressed a plasmid encoding the secretory protein NPY C-terminally tagged with mCherry. NPY-mCherry was prepared by subcloning NPY excised from pEGFP_N1-NPY (a kind gift from Wolf Almers, Oregon Health Sciences University) into pmCherry-N1 (Invitrogen/ThermoFisher). GRINCH cells were subjected to siRNA-mediated knockdown and transfection with NPY-mCherry sequentially. Thus, after 48 h of knockdown, cells

were resuspended and transfected with NPY-mCherry by Amaxa nucleofection and then replated and used for experiments at 72 h after the knockdown was initiated. For testing phenotypic rescue of cells expressing GFP-G1 or GFP-G1(K124), cells were transfected with the plasmid concurrent with siRNA-mediated knockdown using the RNAiMax reverse transfection procedure, with increased lipofectamine. Cells were used for experimentation at 48 h.

Generation of GFP-ABCG1 and a nonfunctional mutant
Mouse ABCG1 cDNA in pcDNA3.1 (obtained from the Hedrick Laboratory, LaJolla Institute of Allergy and Immunology) was used to generate N-terminally EGFP-tagged ABCG1 (GFP-G1) by insertion into pmEGFP_C1 (Invitrogen/ThermoFisher). Use of N-terminal tagging was based on a previous strategy (Vaughan, 2005). The sequence was confirmed, and the construct was transfected into INS1 823/13 cells using Amaxa. Expressing cells were selected for neomycin resistance and small clones were isolated for subsequent propagation using cloning rings. Clonal isolation was validated by fluorescence microscopy, and cells were maintained as for parent INS1 cells except in the continued presence of neomycin. To generate a mutant of ABCG1 that does not exhibit altered membrane trafficking but is inactive for cholesterol efflux, we followed a previous strategy (Gao et al., 2012). Residue K124 in the Walker A motif in the mouse sequence (corresponding to K120 in human ABCG1 [Gao et al., 2012]) was changed to M in our GFP-G1 construct using quick-change mutagenesis to create GFP-G1(K124M). The mutation was verified by sequencing, and the construct was expressed in INS1 823/13 cells using electroporation and selected for neomycin resistance. Lower-level expressing cells were selected by fluorescence-activated cell sorting (FACS).

Procedure for ELISA
Cell-associated insulin (extracted in 1% Triton, 10 mM Tris, 100 mM NaCl, proteinase inhibitors with 1 min bath sonication) and secreted insulin were assayed by enzyme-linked immunosorbent assay (ELISA) using a homemade kit. An anti-rat proinsulin/insulin Mab (Meridian Life Science E86201M) was used to coat the plates; anti-rat insulin antibody (Millipore 1013K) was used as sandwich antibody; and insulin standards were Millipore 8013-K.

Western blotting
For quantitative Western blotting, samples containing equal protein (BCA assay) or equal fraction of total (for cell fractionation) were electrophoresed on NuPAGE 4–12% Bis-Tris gels (Invitrogen/ThermoFisher) and transferred to nitrocellulose. Blotting with primary and secondary antibodies was done in 2.5% milk in phosphate-buffered saline (PBS) 0.1% Tween20. Secondary antibodies conjugated to either horseradish peroxidase or infrared (Licor) were used for detection; dilutions for Licor secondary reagents were 1:10,000 for goat anti-rabbit 696 and donkey anti-goat 800 and 1:25,000 for goat anti-mouse 800. Quantitative densitometry of saved Tiff images was done using Fujifilm Multi Gauge software. All cell lysate samples were also blotted for γ-adaptin to ensure normalization between different samples on blots. We justified use of γ-adaptin for this purpose by showing that the γ-adaptin/actin ratio was constant in all types of cell lysate samples.

Subcellular fractionation of GRINCH cells
We devised an isoosmotic procedure capable of resolving organelles (e.g., TGN, immature, mature granules) having minor differences in buoyant density. Cells suspended in 0.29 M sucrose, 5 mM MOPS,

0.2 mM EDTA (pH 7.2) supplemented with protease inhibitor cocktail (Complete Mini, Roche) were homogenized using a ball bearing homogenizer (0.2507-in. cylinder; Balch and Rothman, 1985) eight passes with 0.2496-in. ball bearing. The homogenate was spun $1000 \times g$, 10 min, in a microcentrifuge to prepare a postnuclear fraction, which was then mixed with 60% Percoll in homogenization medium to give a final Percoll concentration of 32% (refractive index $n = 1.3541$). The resulting solution was spun 40 min at $35,000 \times g$ in a tabletop ultracentrifuge using a Beckman TLA120.2 rotor. The upper 1/2 of the Percoll solution in each tube was collected to provide material enriched in lower-density organelles and the lower ¼–⅓ of the solution above the Percoll pellet was collected to provide material enriched in higher-density organelles including granules. Each of these fractions was diluted 1:1 with homogenization medium and layered over a step gradient of 15 and 30% Optiprep, each layer containing 5 mM MOPS, 0.2 mM EDTA, and sufficient sucrose to maintain isoosmolarity. These upper and lower samples were spun 2.5 h, 45,000 rpm, in a Beckman SW55 rotor to generate fractions U1 and L1 at the load/15% Optiprep interface and U2 and L2 at the 15%/30% Optiprep interface, respectively. U1, U2, L1, and L2 were each diluted with homogenization medium and spun 60,000 rpm in the TLA120.2 rotor to recover the fractions above small amounts of residual Percoll. The procedure is summarized in Figure 1C along with the distributions of organelle markers and SfGFP-labeled proteins determined by Western blotting.

For additional comparison of the levels of selected secretory and membrane proteins in control and ABCG1-deficient cell samples, postnuclear supernatant fractions prepared as above were loaded on continuous (0.6–1.6 M) sucrose gradients prepared in Beckman SW41 tubes and spun overnight (≥16 h, 35,000 rpm). Sucrose solutions contained MOPS, EDTA, and protease inhibitors as above. Fractions collected manually were individually checked for refractive index (to confirm near identity of gradients being compared), diluted with 0.15 M MOPS, pelleted (40 min, 60,000 rpm) in a TLA120.2 rotor, resuspended and solubilized in sample buffer for Western blotting. An equal fraction of the total amount of each gradient fraction was run on the gel. Alongside the gradient fractions derived from control and ABCG1 knockdown cells that were run on individual gels, additional identical samples were run on each of the gels to enable normalization and thus quantitative comparison between the different blots.

Pulse-chase biosynthetic labeling and immunoadsorption
GRINCH cells subjected to RNAi-mediated knockdown and plating as described above were preincubated 30 min in cysteine- and methionine-free RPMI medium containing 1.0 mg/ml bovine serum albumin (BSA), pulse labeled 30 min in the same medium containing ^{35}S Easy Tag Express Protein Labeling Mix (Perkin Elmer NEG772014; 80–100 µCi/ml) and then washed and chase incubated in low glucose (5.5 mM) DMEM containing 2 mM glutamine and 1% FBS. Individual wells were used for each timepoint and media were removed and spun in a microcentrifuge to clear any cellular debris. Cells were washed twice with PBS, lysed 20 min on ice with lysis buffer (1% Triton X-100, 10 mM Tris, 100 mM NaCl, 1 mM EDTA plus proteinase inhibitors), and cleared of debris by centrifugation. An aliquot of each supernatant was used to measure protein and another aliquot was diluted with RIPA buffer and preadsorbed with Protein G-Sepharose 30 min at 4°C and then used for immunoadsorption overnight at 4°C with mouse anti-GFP/Protein G-Sepharose. The amounts of anti-GFP sufficient to adsorb all radiolabeled pro/insulin or SfGFP-labeled protein were determined by initial titrations. Following three washes with 1% Triton containing lysis buffer and

once with PBS, immunoadsorbed label was solubilized in sample buffer and resolved by SDS–PAGE on 4–12% Bis-Tris gels. After fixation in isopropanol-acetic acid, the gels were dried and used for phosphorimaging and quantification using the Fujifilm Multi Gauge program. In one set of experiments, the proteasomal inhibitor MG132 was added (10 µM final) during prepulse and pulse incubations to test its effect on newly synthesized proinsulin. All further processing was as above.

GFP fluorescence assay of secretion

To capitalize on the stable expression of hPro-CpepSfGFP in GRINCH cells, we devised an easy and sensitive assay of secretion based on quantification of GFP fluorescence. (This resembles a previous assay used to monitor SfGFP secretion from transfected mouse pancreatic islets [Zhu *et al.*, 2016].) In our experiments, cells were knocked down and seeded at 1×10^6 cells/well in six-well plates and cultured in RPMI–10% FBS. When tested, soluble cholesterol (20 µM MβCD-cholesterol) or MβCD alone was added in the same medium on the final day of the 3-d knockdown ~20 h before starting the experiment. Before testing secretion, cells were preincubated 4 h in KRBH-0.5% BSA medium containing 3 mM glucose, then incubated 1 h in the same medium to provide basal secretion, and then switched to KRBH-0.5% BSA containing 20 mM glucose for a 30-min stimulation. Media following basal and stimulated secretion were each collected and centrifuged at 10,000 rpm for 4 min to pellet any debris and dislodged cells. Cells following stimulation were washed, scraped, and pelleted from PBS (10,000 rpm, 4 min), lysed and solubilized in 1% Triton, 10 mM Tris, 100 mM NaCl, 1 mM EDTA plus proteinase inhibitors, and centrifuged at 13,000 rpm, 4 min, and the supernatant used for assaying GFP fluorescence (alongside media samples), protein, and Western blotting to determine the extent of knockdown. Fluorescence at 510 nm (emission peak of SfGFP) recorded in a fluorimeter (Fluorolog 3, model FL3-21 from Horiba) was used to calculate fractional secretion (percent of total GFP fluorescence secreted under basal and stimulated conditions). Within each experiment, control knockdowns were performed in duplicate wells and ABCG1 and OSBP knockdowns were each performed in triplicate wells.

Assays of free cholesterol and of cholesterol synthesis

To determine free cholesterol content, cell samples were scraped and harvested from six-well plates in PBS and were aliquoted for protein assay (used for normalization), Western blotting (to confirm RNAi-mediated knockdown), and lipid extraction (procedure of Bligh and Dyer, 1959). The dried chloroform phases were dissolved in isopropanol-NP40 (9:1 vol/vol) and assayed for cholesterol fluorimetrically using enzymatic oxidation by cholesterol oxidase and detection via coupled horseradish peroxidase and Amplex Red (Robinet *et al.*, 2010).

To assay cholesterol biosynthesis, we adapted a previously published procedure (Yamauchi *et al.*, 2015). Cells in six-well plates were preincubated 30 min in RPMI 1640 medium containing 1 mg/ml BSA and then labeled 2 h with 20 µCi/ml [³H]acetate (Perkin Elmer; NET003H) in the same medium. Following washing and scraping in PBS, aliquots of cell suspension were used as described above (see free cholesterol assay). Extracted and dried lipids were dissolved in 1:1 chloroform/methanol containing unlabeled cholesterol standard and subjected to TLC on silica gel plates developed in hexane/ethyl ether/acetic acid (90:10:1). Cholesterol located by iodine vapor was scraped and counted in a scintillation counter. The amount of [³H] cholesterol was normalized to protein.

Fluorescence and immunofluorescence microscopy

All microscopy was performed on cells that had been fixed with 3% formaldehyde in 0.1 M sodium phosphate for 45 min at room temperature. For immunostaining, the samples were further processed at room temperature by quenching in 50 mM glycine in PBS, permeabilization in 0.1% Triton X-100 in PBS, and blocking in 2% goat serum in the permeabilization medium. Staining with primary antibodies and secondary antibodies diluted in blocking medium was carried out for 1 h and 45 min, respectively, with intervening washes in permeabilization medium.

After staining, samples were washed in permeabilization medium and finally in PBS before being mounted in Prolong Gold Antifade (Invitrogen/ThermoFisher). Coverslips were imaged using a Nikon C1 laser scanning confocal unit attached to a Nikon Eclipse TE2000-E microscope with a 100×, 1.45-NA (numerical aperture) Plan Apochromat objective. Image analysis was preformed using ImageJ.

In the experiment presented in Figure 6D, we analyzed the extent to which SfGFP overlapped with the TGN marker Golgin97 in control and OSBP knockdown cells. For this purpose, we used NIS-Elements Software (Nikon) to manually define regions of interest (ROI) on confocal images that were marked by concentrated Golgin 97 signal, and we quantified the extent to which the SfGFP signal coincided using Manders' overlap.

To detect and analyze relative levels of cholesterol within cells, we followed a recommendation described by Maxfield and Wustner (2012) and stained cells that had been fixed with 3% formaldehyde and quenched with 50 mM glycine using filipin (diluted 1:100 in 5% goat serum in PBS from a 50 mg/ml stock in dry dimethyl sulfoxide). Staining and subsequent processing were performed in a darkened room. Slides were mounted in Prolong Gold Antifade (as above). Images were recorded using a wide-field Nikon TE-2000 fluorescence microscope (100× objective, 4′,6-diamidino-2-phenylindole [DAPI] filters). Because filipin fluorescence readily bleaches upon excitation, we focused our images using the fluorescence from SfGFP and then switched to the DAPI filter set for immediate image recording. Filipin intensities in ROI were measured, normalized, and analyzed using strategies employed by Mesmin *et al.* (2017) as indicated under *Results*.

Statistical analyses

Data were analyzed using statistical software in GraphPad Prism 7. The number of biological replicates/separate experiments (*n*) and specific statistical tests used are indicated in the figure legends. Where cells were analyzed in fluorescent images, the number of cells is indicated by #. Although we evaluated statistical significance comprehensively among different samples within experiments, we have identified significance in the figures for comparisons that are specifically relevant to the experiments' goals. In all figures, *, $p < 0.05$; **, $p < 0.01$; ***, $p < 0.001$; ****, $p < 0.0001$; brackets identify samples being compared except where comparisons are to the control, in which case p values are given without brackets. All results with error bars are presented as mean ± SEM.

REFERENCES

Ahras M, Otto GP, Tooze SA (2006). Synaptotagmin IV is necessary for the maturation of secretory granules in PC12 cells. J Cell Biol 173, 241–251.

Ansari I-UH, Longacre MJ, Paulusma CC, Stoker SW, Kendrick MA, MacDonald MJ (2015). Characterization of P4 ATPase phospholipid translocases (flippases) in human and rat pancreatic beta cells: their gene silencing inhibits insulin secretion. J Biol Chem 290, 23110–23123.

Arnaoutova I, Jackson CL, Al-Awar OS, Donaldson JG, Loh YP (2003). Recycling of Raft-associated prohormone sorting receptor carboxypeptidase E requires interaction with ARF6. Mol Biol Cell 14, 4448–4457.

Bäck N, Rajagopal C, Mains RE, Eipper BA (2010). Secretory granule membrane protein recycles through multivesicular bodies. Traffic 11, 972–986.

Balch WE, Rothman JE (1985). Characterization of protein transport between successive compartments of the Golgi apparatus: asymmetric properties of donor and acceptor activities in a cell-free system. Arch Biochem Biophys 240, 413–425.

Bauer RA, Overlease RL, Lieber JL, Angleson JK (2004). Retention and stimulus-dependent recycling of dense core vesicle content in neuroendocrine cells. J Cell Sci 117, 2193–2202.

Blazquez M, Thiele C, Huttner WB, Docherty K, Shennan KIJ (2000). Involvement of the membrane lipid bilayer in sorting prohormone convertase 2 into the regulated secretory pathway. Biochem J 349, 843–852.

Bligh EG, Dyer WJ (1959). A rapid method of total lipid extraction and purification. Can J Biochem Physiol 37, 911–917.

Bogan JS, Xu Y, Hao M (2012). Cholesterol accumulation increases linsulin granule size and impairs membrane trafficking. Traffic 13, 1466–1480.

Brunham LR, Kruit JK, Pape TD, Timmins JM, Reuwer AQ, Vasanji Z, Marsh BJ, Rodrigues B, Johnson JD, Parks JS, et al. (2007). β-Cell ABCA1 influences insulin secretion, glucose homeostasis and response to thiazolidinedione treatment. Nat Med 13, 340–347.

Cao M, Mao Z, Kam C, Xiao N, Cao X, Shen C, Cheng KY, Xu A, Lee K, Jiang L, et al. (2013). PICK1 and ICA69 control insulin granule trafficking and their deficiencies lead to impaired glucose tolerance. PLoS Biol 11, e1001541.

Chang T-Y, Chang CCY, Ohgami N, Yamauchi Y (2006). Cholesterol sensing, trafficking, and esterification. Annu Rev Cell Dev Biol 22, 129–157.

Devlin C, Pipalia NH, Liao X, Schuchman EH, Maxfield FR, Tabas I (2010). Improvement in lipid and protein trafficking in Niemann-Pick C1 cells by correction of a secondary enzyme defect. Traffic 11, 601–615.

Dhanvantari S, Loh YP (2000). Lipid raft association of carboxypeptidase E is necessary for its function as a regulated secretory pathway sorting receptor. J Biol Chem 275, 29887–29893.

Du W, Zhou M, Zhao W, Cheng D, Wang L, Li J, Song E, Feng W, Xue Y, Xu P, et al. (2016). HID-1 is required for homotypic fusion of immature secretory granules during maturation. eLife 5, e18134.

Duncan RR, Greaves J, Wiegand UK, Matskevich I, Bodammer G, Apps DK, Shipston MJ, Chow RH (2003). Functional and spatial segregation of secretory vesicle pools according to vesicle age. Nature 422, 176–180.

Edwards SL, Charlie NK, Richmond JE, Hegermann J, Eimer S, Miller KG (2009). Impaired dense core vesicle maturation in Caenorhabditis elegans mutants lacking Rab2. J Cell Biol 186, 881–895.

Frechin M, Stoeger T, Daetwyler S, Gehin C, Battich N, Damm E-M, Stergiou L, Riezman H, Pelkmans L (2015). Cell-intrinsic adaptation of lipid composition to local crowding drives social behaviour. Nature 523, 88–91.

Gao X, Gu H, Li G, Rye K-A, Zhang D-W (2012). Identification of an amino acid residue in ATP-binding cassette transport G1 critical for mediating cholesterol efflux. Biochim Biophys Acta 1821, 552–559.

Goginashvili A, Zhang Z, Erbs E, Spiegelhalter C, Kessler P, Mihlan M, Pasquier A, Krupina K, Schieber N, Cinque L, et al. (2015). Insulin secretory granules control autophagy in pancreatic β cells. Science 347, 878–882.

Goldstein JL, Brown MS (2015). A century of cholesterol and coronaries: from plaques to genes to statins. Cell 161, 161–172.

Gondre-Lewis MC (2006). Abnormal sterols in cholesterol-deficiency diseases cause secretory granule malformation and decreased membrane curvature. J Cell Sci 119, 1876–1885.

Grimmer SMY, Walchli S, van Deurs B, Sandvig K (2005). Golgi vesiculation induced by cholesterol occurs by a dynamin- and cPLA-dependent mechanism. Traffic 6, 144–156.

Grishanin RN, Klenchin VA, Loyet KM, Kowalchyk JA, Ann K, Martin TFJ (2002). Membrane association domains in Ca²⁺-dependent activator protein for secretion mediate plasma membrane and dense-core vesicle binding required for Ca²⁺-dependent exocytosis. J Biol Chem 277, 22025–22034.

Haataja L, Snapp E, Wright J, Liu M, Hardy AB, Wheeler MB, Markwardt ML, Rizzo M, Arvan P (2013). Proinsulin intermolecular interactions during secretory trafficking in pancreatic cells. J Biol Chem 288, 1896–1906.

Halban PA, Wolheim CB (1980). Intracellular degradation of insulin stores by rat pancreatic islets in vitro. J Biol Chem 255, 6003–6006.

Hammarlund M, Watanabe S, Schuske K, Jorgensen EM (2008). CAPS and syntaxin dock dense core vesicles to the plasma membrane in neurons. J Cell Biol 180, 483–491.

Hankins HM, Sero YY, Diab NS, Menon AK, Graham TR (2015). Phosphatidylserine translocation at the yeast trans-Golgi network regulates protein sorting into exocytic vesicles. Mol Biol Cell 26, 4674–4685.

Hannemann M, Sasidharan N, Hegermann J, Kutscher LM, Koenig S, Eimer S (2012). TBC-8, a putative RAB-2 GAP, regulates dense core vesicle maturation in Caenorhabditis elegans. PLoS Genet 8, e1002722.

Hao M, Bogan JS (2009). Cholesterol regulates glucose-stimulated insulin secretion through phosphatidylinositol 4,5-bisphosphate. J Biol Chem 284, 29489–29498.

Hao M, Head WS, Gunawardana SC, Hasty AH, Piston DW (2007). Direct effect of cholesterol on insulin secretion: a novel mechanism for pancreatic-cell dysfunction. Diabetes 56, 2328–2338.

Hohmeier HE, Mulder H, Chen G, Henkel-Rieger R, Prentki M, Newgard CB (2000). Isolation of INS-1-derived cell lines with robust ATP-sensitive K+ channel-dependent and -independent glucose-stimulated insulin secretion. Diabetes 49, 424–430.

Holst B, Madsen KL, Jansen AM, Jin C, Rickhag M, Lund VK, Jensen M, Bhattia V, Sorensen G, Madsen AN, et al. (2013). PICK1 deficiency impairs secretory vesicle biogenesis and leads to growth retardation and decreased glucose tolerance. PLoS Biol 11, e1001542.

Holthuis JCM, Menon AK (2014). Lipid landscapes and pipelines in membrane homeostasis. Nature 510, 48–57.

Hosaka M (2003). Secretogranin III binds to cholesterol in the secretory granule membrane as an adapter for chromogranin A. J Biol Chem 279, 3627–3634.

Hosaka M (2005). Interaction between secretogranin III and carboxypeptidase E facilitates prohormone sorting within secretory granules. J Cell Sci 118, 4785–4795.

Hummer BH, de Leeuw NF, Burns C, Chen L, Joens MS, Hosford B, Fitzpatrick JAJ, Asensio CS (2017). HID-1 controls formation of large dense core vesicles by influencing cargo sorting and trans-Golgi network acidification. Mol Biol Cell 28, 3870–3880.

Ito A, Hong C, Rong X, Zhu X, Tarling EJ, Hedde PN, Gratton E, Parks J, Tontonoz P (2015). LXRs link metabolism to inflammation through Abca1-dependent regulation of membrane composition and TLR signaling. eLife 4, e08009.

Kabachinski G, Kielar-Grevstad DM, Zhang X, James DJ, Martin TF J (2016). Resident CAPS on dense-core vesicles docks and primes vesicles for fusion. Mol Biol Cell 27, 654–668.

Kanerva K, Uronen R-L, Blom T, Li S, Bittman R, Lappalainen P, Peränen J, Raposo G, Ikonen E (2013). LDL cholesterol recycles to the plasma membrane via a Rab8a-myosin5b-actin-dependent membrane transport route. Dev Cell 27, 249–262.

Klemm RW, Ejsing CS, Surma MA, Kaiser HJ, Gerl MJ, Sampaio JL, de Robillard Q, Ferguson C, Proszynski TJ, Shevchenko A, Simons K (2009). Segregation of sphingolipids and sterols during formation of secretory vesicles at the trans-Golgi network. J Cell Biol 185, 601–612.

Klumperman J, Kuliawat R, Griffith JM, Geuze HJ, Arvan P (1998). Mannose 6-phosphate receptors are sorted from immature secretory granules via

adaptor protein AP-1, clathrin, and syntaxin 6-positive vesicles. J Cell Biol 141, 359–371.

Kobayashi A (2006). Efflux of sphingomyelin, cholesterol, and phosphatidylcholine by ABCG1. J Lipid Res 47, 1791–1802.

Kreutzberger AJB, Kiessling V, Tamm LK (2015). High cholesterol obviates a prolonged hemifusion intermediate in fast SNARE-mediated membrane fusion. Biophys J 109, 319–329.

Kruit JK, Wijesekara N, Fox JE, Dai XQ, Brunham LR, Searle GJ, Morgan GP, Costin AJ, Tang R, Bhattacharjee A, et al. (2011). Islet cholesterol accumulation due to loss of ABCA1 leads to impaired exocytosis of insulin granules. Diabetes 60, 3186–3196.

Kruit JK, Wijesekara N, Westwell-Roper C, Vanmierlo T, de Haan W, Bhattacharjee A, Tang R, Wellington CL, LütJohann D, Johnson JD, et al. (2012). Loss of both ABCA1 and ABCG1 results in increased disturbances in islet sterol homeostasis, inflammation, and impaired-cell function. Diabetes 61, 659–664.

Kuliawat R, Arvan P (1992). Protein targeting via the "constitutive-like" secretory pathway in isolated pancreatic islets: passive sorting in the immature granule compartment. J Cell Biol 118, 521–529.

Kuliawat R, Arvan P (1994). Distinct molecular mechanisms for protein sorting within immature secretory granules of pancreatic beta-cells. J Cell Biol 126, 77–86.

Kuliawat R, Kalina E, Bock J, Fricker L, McGraw TE, Kim SR, Zhong J, Scheller R, Arvan P (2004). Syntaxin-6 SNARE involvement in secretory and endocytic pathways of cultured pancreatic β-cells. Mol Biol Cell 15, 1690–1701.

Liu Y, Schirra C, Edelmann L, Matti U, Rhee J, Hof D, Bruns D, Brose N, Rieger H, Stevens DR, et al. (2010). Two distinct secretory vesicle–priming steps in adrenal chromaffin cells. J Cell Biol 190, 1067–1077.

Marsh BJ, Soden C, Alarcón C, Wicksteed BL, Yaekura K, Costin AJ, Morgan GP, Rhodes CJ (2007). Regulated autophagy controls hormone content in secretory-deficient pancreatic endocrine β-cells. Mol Endocrinol 21, 2255–2269.

Matsunaga K, Taoka M, Isobe T, Izumi T (2017). Rab2a and Rab27a cooperatively regulate the transition from granule maturation to exocytosis through the dual effector Noc2. J Cell Sci 130, 541–550.

Maxfield FR, Wüstner D (2012). Analysis of cholesterol trafficking with fluorescent probes. Methods Cell Biol 108, 367–393.

Mesmin B, Antonny B, Drin G (2013a). Insights into the mechanisms of sterol transport between organelles. Cell Mol Life Sci 70, 3405–3421.

Mesmin B, Bigay J, Moser von Filseck J, Lacas-Gervais S, Drin G, Antonny B (2013b). A four-step cycle driven by PI(4)P hydrolysis directs sterol/PI(4)P exchange by the ER-Golgi tether OSBP. Cell 155, 830–843.

Mesmin B, Bigay J, Polidori J, Jamecna D, Lacas-Gervais S, Antonny B (2017). Sterol transfer, PI4P consumption, and control of membrane lipid order by endogenous OSBP. EMBO J 36, 3156–3174.

Mesmin B, Maxfield FR (2009). Intracellular sterol dynamics. Mol Cell Biol Lipids 1791, 636–645.

Michael DJ, Xiong W, Geng X, Drain P, Chow RH (2007). Human insulin vesicle dynamics during pulsatile secretion. Diabetes 56, 1277–1288.

Mobius W, van Donselaar E, Ohno-Iwashita Y, Shimada Y, Heijnen HFG, Slot JW, Geuze HJ (2003). Recycling compartments and the internal vesicles of multivesicular bodies harbor most of the cholesterol found in the endocytic pathway. Traffic 4, 222–231.

Nilsson I, Ohvo-Rekilä H, Slotte JP, Johnson AE, Heijne von G (2001). Inhibition of protein translocation across the endoplasmic reticulum membrane by sterols. J Biol Chem 276, 41748–41754.

Nishimura T, Uchida Y, Yachi R, Kudlyk T, Lupashin V, Inoue T, Taguchi T, Arai H (2013). Oxysterol-binding protein (OSBP) is required for the perinuclear localization of intra-Golgi v-SNAREs. Mol Biol Cell 24, 3534–3544.

Oliver C, Hand AR (1983). Enzyme modulation of the Golgi apparatus and GERL: a cytochemical study of parotid acinar cells. J Histochem Cytochem 31, 1041–1048.

Orci L, Montesano R, Meda P, Malaisse-Lagae F, Brown D, Perrelet A, Vassalli P (1981). Heterogeneous distribution of filipin–cholesterol complexes across the cisternae of the Golgi apparatus. Proc Natl Acad Sci USA 78, 293–297.

Orci L, Ravazzola M, Amherdt M, Yanaihara C, Yanaihara N, Halban PA, Renold AE, Perrelet A (1984). Insulin, not C-peptide (Proinsulin), is present in crinophagic bodies of the pancreatic B-cell. J Cell Biol 98, 222–228.

Peretti D, Dahan N, Shimoni E, Hirschberg K, Lev S (2008). Coordinated lipid transfer between the endoplasmic reticulum and the Golgi complex requires the VAP proteins and is essential for Golgi-mediated transport. Mol Biol Cell 19, 3871–3884.

Perry RJ, Ridgway ND (2006). Oxysterol-binding protein and vesicle-associated membrane protein-associated protein are required for sterol-dependent activation of the ceramide transport protein. Mol Biol Cell 17, 2604–2616.

Phillips MC (2014). Molecular mechanisms of cellular cholesterol efflux. J Biol Chem 289, 24020–24029.

Pomorski T, Holthuis JCM, Herrmann A, van Meer G (2004). Tracking down lipid flippases and their biological functions. J Cell Sci 117, 805–813.

Quazi F, Molday RS (2013). Differential phospholipid substrates and directional transport by ATP-binding cassette proteins ABCA1, ABCA7, and ABCA4 and disease-causing mutants. J Biol Chem 288, 34414–34426.

Rhodes CJ, Halban PA (1987). Newly synthesized proinsulin/insulin and stored insulin are released from pancreatic B cells predominantly via a regulated, rather than a constitutive, pathway. J Cell Biol 105, 145–153.

Riahi Y, Wikstrom JD, Bachar-Wikstrom E, Polin N, Zucker H, Lee MS, Quan W, Haataja L, Liu M, Arvan P, et al. (2016). Autophagy is a major regulator of beta cell insulin homeostasis. Diabetologia 59, 1480–1491.

Robinet P, Wang Z, Hazen SL, Smith JD (2010). A simple and sensitive enzymatic method for cholesterol quantification in macrophages and foam cells. J Lipid Res 51, 3364–3369.

Rorsman P, Renström E (2003). Insulin granule dynamics in pancreatic beta cells. Diabetologia 46, 1029–1045.

Sano O, Kobayashi A, Nagao K, Kumagai K, Kioka N, Hanada K, Ueda K, Matsuo M (2007). Sphingomyelin-dependence of cholesterol efflux mediated by ABCG1. J Lipid Res 48, 2377–2384.

Sato T, Herman L (1981). Stereological analysis of normal rabbit pancreatic islets. Am J Anat 161, 71–84.

Schuit FC, In't Veld PA, Pipeleers DG (1988). Glucose stimulates proinsulin biosynthesis by a dose-dependent recruitment of pancreatic beta cells. Proc Natl Acad Sci USA 85, 3865–3869.

Sirkis DW, Edwards RH, Asensio CS (2013). Widespread dysregulation of peptide hormone release in mice lacking adaptor protein AP-3. PLoS Genet 9, e1003812.

Sokolov A, Radhakrishnan A (2010). Accessibility of cholesterol in endoplasmic reticulum membranes and activation of SREBP-2 switch abruptly at a common cholesterol threshold. J Biol Chem 285, 29480–29490.

Solimena M, Dirkx R, Hermel JM, Pleasic-Williams S, Shapiro JA, Caron L, Rabin DU (1996). ICA 512, an autoantigen of type I diabetes, is an intrinsic membrane protein of neurosecretory granules. EMBO J 15, 2102–2114.

Speidel D, Salehi A, Obermueller S, Lundquist I, Brose N, Renström E, Rorsman P (2008). CAPS1 and CAPS2 regulate stability and recruitment of insulin granules in mouse pancreatic β cells. Cell Metab 7, 57–67.

Storey MK, Byers DM, Cook HW, Ridgway ND (1998). Cholesterol regulates oxysterol binding protein (OSBP) phosphorylation and Golgi localization in Chinese hamster ovary cells: correlation with stimulation of sphingomyelin synthesis by 25-hydroxycholesterol. Biochem J 336(Pt 1), 247–256.

Sturek JM, Castle JD, Trace AP, Page LC, Castle AM, Evans-Molina C, Parks JS, Mirmira RG, Hedrick CC (2010). An intracellular role for ABCG1-mediated cholesterol transport in the regulated secretory pathway of mouse pancreatic β cells. J Clin Invest 120, 2575–2589.

Sumakovic M, Hegermann J, Luo L, Husson SJ, Schwarze K, Olendrowitz C, Schoofs L, Richmond J, Eimer S (2009). UNC-108/RAB-2 and its effector RIC-19 are involved in dense core vesicle maturation in Caenorhabditis elegans. J Cell Biol 186, 897–914.

Tarling EJ, Edwards PA (2011). ATP binding cassette transporter G1 (ABCG1) is an intracellular sterol transporter. Proc Natl Acad Sci USA 108, 19719–19724.

Tarling EJ, Edwards PA (2012). Dancing with the sterols: critical roles for ABCG1, ABCA1, miRNAs, and nuclear and cell surface receptors in controlling cellular sterol homeostasis. Biochim Biophys Acta 1821, 386–395.

Topalidou I, Cattin-Ortolá J, Pappas AL, Cooper K, Merrihew GE, MacCoss MJ, Ailion M (2016). The EARP complex and its interactor EIPR-1 are required for cargo sorting to dense-core vesicles. PLoS Genet 12, e1006074.

Tsuchiya M, Hosaka M, Moriguchi T, Zhang S, Suda M, Yokota-Hashimoto H, Shinozuka K, Takeuchi T (2010). Cholesterol biosynthesis pathway intermediates and inhibitors regulate glucose-stimulated insulin secretion and secretory granule formation in pancreatic β-cells. Endocrinology 151, 4705–4716.

Turner MD, Arvan P (2000). Protein traffic from the secretory pathway to the endosomal system in pancreatic β-cells. J Biol Chem 275, 14225–14230.

van Meer G, Voelker DR, Feigenson GW (2008). Membrane lipids: where they are and how they behave. Nat Rev Mol Cell Biol 9, 112–124.

Vaughan AM (2003). ABCA1 redistributes membrane cholesterol independent of apolipoprotein interactions. J Lipid Res 44, 1373–1380.

Vaughan AM (2005). ABCG1 redistributes cell cholesterol to domains removable by high density lipoprotein but not by lipid-depleted apolipoproteins. J Biol Chem 280, 30150–30157.

Vo YP, Hutton JC, Angleson JK (2004). Recycling of the dense-core vesicle membrane protein phogrin in Min6 β-cells. Biochem Biophys Res Commun 324, 1004–1010.

Walter AM, Kurps J, de Wit H, Schöning S, Toft-Bertelsen TL, Lauks J, Ziomkiewicz I, Weiss AN, Schulz A, Fischer von Mollard G, et al. (2014). The SNARE protein vti1a functions in dense-core vesicle biogenesis. EMBO J 33, 1681–1697.

Wang X, Collins HL, Ranalletta M, Fuki IV, Billheimer JT, Rothblat GH, Tall AR, Rader DJ (2007). Macrophage ABCA1 and ABCG1, but not SR-BI, promote macrophage reverse cholesterol transport in vivo. J Clin Invest 117, 2216–2224.

Wang Y, Thiele C, Huttner WB (2000). Cholesterol is required for the formation of regulated and constitutive secretory vesicles from the trans-Golgi network. Traffic 1, 952–962.

Wasmeier C, Burgos PV, Trudeau T, Davidson HW, Hutton JC (2005). An extended tyrosine-targeting motif for endocytosis and recycling of the dense-core vesicle membrane protein phogrin. Traffic 6, 474–487.

Wasmeier C, Hutton JC (1996). Molecular cloning of phogrin, a protein-tyrosine phosphatase homologue localized to insulin secretory granule membrane. J Biol Chem 271, 18162–18170.

Westhead EW (1987). Lipid composition and orientation in secretory vesicles. Ann NY Acad Sci 493, 92–100.

Wicksteed B, Alarcon C, Briaud I, Lingohr MK, Rhodes CJ (2003). Glucose-induced translational control of proinsulin biosynthesis is proportional to preproinsulin mRNA levels in islet-cells but not regulated via a positive feedback of secreted insulin. J Biol Chem 278, 42080–42090.

Xia F, Xie L, Mihic A, Gao X, Chen Y, Gaisano HY, Tsushima RG (2008). Inhibition of cholesterol biosynthesis impairs insulin secretion and voltage-gated calcium channel function in pancreatic β-cells. Endocrinology 149, 5136–5145.

Yamauchi Y, Iwamoto N, Rogers MA, Abe-Dohmae S, Fujimoto T, Chang CCY, Ishigami M, Kishimoto T, Kobayashi T, Ueda K, et al. (2015). Deficiency in the lipid exporter ABCA1 impairs retrograde sterol movement and disrupts sterol sensing at the endoplasmic reticulum. J Biol Chem 290, 23464–23477.

Zachowski A, Henry JP, Devaux PF (1989). Control of transmembrane lipid asymmetry in chromaffin granules by an ATP-dependent protein. Nature 340, 75–76.

Zhang X, Jiang S, Mitok KA, Li L, Attie AD, Martin TFJ (2017). BAIAP3, a C2 domain-containing Munc13 protein, controls the fate of dense-core vesicles in neuroendocrine cells. J Cell Biol 4, jcb.201702099.

Zhu S, Larkin D, Lu S, Inouye C, Haataja L, Anjum A, Kennedy R, Castle D, Arvan P (2016). Monitoring C-peptide storage and secretion in islet β-cells in vitro and in vivo. Diabetes 65, 699–709.

Zhu X, Lee JY, Timmins JM, Brown JM, Boudyguina E, Mulya A, Gebre AK, Willingham MC, Hiltbold EM, Mishra N, et al. (2008). Increased cellular free cholesterol in macrophage-specific Abca1 knock-out mice enhances pro-inflammatory response of macrophages. J Biol Chem 283, 22930–22941.